International Journal of Climatology

International Journal of Climatology | RMetS

RESEARCH ARTICLE OPEN ACCESS

How Well Do CMIP6 Models Simulate the Influence of the West African Westerly Jet on Sahel Precipitation?

Akintunde I. Makinde[1] | Babatunde J. Abiodun[1,2] | Rachel James[3,4] | Richard Washington[4] | Ellen Dyer[4] | Tom Webb[4]

[1]Climate Systems Analysis Group, Department of Environmental and Geographical Science, University of Cape Town, Cape Town, South Africa | [2]Nansen-Tutu Centre for Marine Environmental Research, Department of Oceanography, University of Cape Town, Cape Town, South Africa | [3]School of Geographical Sciences, University of Bristol, Bristol, UK | [4]School of Geography and the Environment, University of Oxford, Oxford, UK

Correspondence: Akintunde I. Makinde (mckynde@gmail.com)

Received: 4 May 2025 | **Revised:** 17 December 2025 | **Accepted:** 24 March 2026

Keywords: CMIP6 | low-level jet | moisture transport | Saharan heat low | Sahel | WAWJ | West Africa | west African monsoon | west African westerly jet

ABSTRACT

The West African Westerly Jet (WAWJ) plays a crucial role in Sahel precipitation, yet there is no information on how well the jet and its contribution to Sahel precipitation are simulated in climate models. This study examines the capabilities of Coupled Model Intercomparison Project phase six (CMIP6) models in simulating the WAWJ and its influence on Sahel precipitation. We combine the Climate Research Unit (CRU) observations with the European Centre for Medium-Range Weather Forecast (ECMWF) Atmospheric Reanalysis (ERA5), the Modern-Era Retrospective analysis for Research and Applications, version 2 (MERRA-2) and the National Centres for Environmental Prediction (NCEP) Climate Forecast System Reanalysis version 2 (CFSR-2) to evaluate 25 CMIP6 models. The majority of the models capture the temporal and spatial structure of the jet and agree with ERA5 that the jet features its core at 925 hPa and attains its maximum speed in August. However, the jets form earlier and are stronger in most models than in reanalysis. Although most CMIP6 simulations capture the link between the jet and the temperature distribution over West Africa, they struggle to reproduce the relationship with precipitation, especially over the Sahel. Most simulations fail to replicate the increase in moisture transport (i.e., the eastward and north-eastward transports) associated with stronger WAWJ. Some simulations capture the increased moisture transport but do not translate to increased precipitation over the Sahel. The results of the study show that improving the simulation of Sahel rainfall requires a concerted effort on enhancing the model capability to better represent WAWJ.

1 | Introduction

The high interannual variability of rainfall in the Sahel is a bottleneck to socioeconomic development in the region. The variability fuels extreme events like droughts and floods that usually degrade the environment, damage water resources, induce disease epidemics (e.g., malaria, meningitis), destroy agricultural products (e.g., crops and pasture) and threaten food security in the Sahel (Jnr 2014; Geist and Lambin 2004). The region has a long history of climatic stress from extreme events, including the wet period of the 1930s, 1950s and 1960s (Giannini et al. 2008; Tschakert et al. 2010) and the drought of the 1960s—1990s (Balme et al. 2006). For instance, the Sahelian droughts of 2010 deteriorated the soil quality, destroyed the vegetation (Jnr 2014), put about 10 million people in the communities at risk of acute hunger and caused more than 25% of refugee children in Chad to be malnourished (Vogel 2010). However, the simulation and prediction of rainfall variability over the Sahel remain a big challenge for many climate models (Roehrig et al. 2013; Vellinga et al. 2016), because the rainfall variability is a result of the complex interactions between various atmospheric features (such as African Easterly Jet; AEJ,

Tropical Easterly Jet; TEJ, West African Monsoon; WAM, etc.) in West Africa as well as global ocean–atmosphere interactions. Many climate models struggle to accurately represent these key circulation features and their interactions (Cook and Vizy 2006; Biasutti 2013; Roehrig et al. 2013). Any improvement in the simulation of Sahelian rainfall variability could go a long way in reducing the negative impacts of the variability on socio-economic developments in the Sahel. However, such improvement requires a better understanding of how well the contemporary climate models represent the rainfall-producing features in West Africa.

The West African Westerly Jet (WAWJ), a low-level westerly jet over the eastern Atlantic and the West African coast, is one of the atmospheric features that modulates precipitation over the Sahel. Several studies (e.g., Grodsky et al. 2003; Pu and Cook 2010, 2012; Lele and Leslie 2016; Liu et al. 2020) have documented the characteristics of WAWJ and its moisture transports to West Africa. Pu and Cook (2010) showed that WAWJ is formed through the superposition of the westward extension of the continental thermal low, the West African Heat Low (WAHL) and the Atlantic marine Inter-Tropical Convergence Zone (ITCZ). The climatological WAHL migrates north-westward from its winter position (November–March) to over the Sahara (where it is referred to as the Saharan Heat Low—SHL) during the summer (June–September), just before the climatological monsoon onset (Lavaysse et al. 2009). The SHL's westward extension creates a pressure gradient located between 9° N and 10° N and 20° W and 30° W that speeds up the zonal wind to the east (westerlies; called WAWJ) of the region. The superposition of the large-scale meridional convergence associated with the ITCZ inhibits the formation of meridional acceleration. Pu and Cook (2010) also clearly distinguished the WAWJ from the West African Monsoon (WAM) flow and showed that the jet forms in June and persists into September, reaching maximum velocity exceeding 5.5 ms^{-1} in August. However, Grodsky et al. (2003) showed that in 1999, the jet speed exceeded 15 ms^{-1} at some locations and cooled the sea surface temperature (SST) by about 0.3°C through entrainment and latent heat loss. Liu et al. (2020) and Pu and Cook (2012) showed that WAWJ transports moisture from the eastern Atlantic onto the subcontinent (especially at 8° N–11° N) and has a strong correlation with the interannual variability of the Sahelian rainfall. Liu et al. 2020 also found a strong relationship between the jet and West African precipitation at seasonal and diurnal timescales. Pu and Cook (2010) argued the WAWJ plays a crucial role in the atmosphere–ocean-land surface interactions in West Africa. Hence, reliable simulations and predictions of rainfall in the Sahel may require adequate simulation of WAWJ by the global climate models (GCMs). However, there is a dearth of information on how well the contemporary GCM simulations represent the WAWJ and its influence on precipitation over the Sahel.

Several studies have discussed the shortcomings in the Coupled Model Intercomparison Project CMIP simulations in capturing Sahel rainfall (e.g., Bain et al. 2014; Williams et al. 2015; James et al. 2018; Foltz et al. 2019; Ehsan et al. 2020; Almazroui et al. 2020; Monerie et al. 2020; Dosio et al. 2021; Klutse et al. 2021; Iyakaremye et al. 2021). For example, Monerie et al. (2020) showed that both CMIP5 and CMIP6 simulations underestimate the boreal summer precipitation over the Sahel but overestimate it over the Guinea coast. These biases have been attributed to the inability of the GCMs to simulate the monsoon system and the associated precipitation far enough northward over West Africa (Cook and Vizy 2006; Monerie et al. 2020). The systematic dry bias over the Sahel has also been linked with cold bias over the Sahara (Dixon et al. 2017, 2018; Foltz et al. 2019), a warm bias over the Gulf of Guinea (Roehrig et al. 2013) and a weaker zone of ascent at 10° N in the models (James et al. 2018; Tamoffo et al. 2022). However, despite the strong contributions of WAWJ to the Sahel precipitation (Pu and Cook 2010, 2012; Liu et al. 2020), no studies have investigated the extent to which inadequate simulation of WAWJ in GCMs may contribute to the dry bias over the Sahel rainfall.

The aim of the present study is to examine how well CMIP6 models simulate the characteristics of WAWJ and its influence on the Sahel precipitation. The outline of the paper is as follows. Section 2 presents the methodology, including the description of the study domain, datasets and data analysis methods. Section 3 presents and discusses the results of the analysis, whereas Section 4 gives the concluding remarks.

2 | Methodology

2.1 | Study Domain

The study region is West Africa (4° N—20° N and 20° W—20° E) but with a focus on the Sahel (12° N—20° N and 20° W—20° E) (Figure 1). The Sahel, a semi-arid region in West Africa, stretches from the Atlantic Ocean eastward through northern Senegal, southern Mauritania, the great bend of the Niger River in Mali, Burkina Faso, southern Niger, northeastern Nigeria, south-central Chad and into Sudan. It forms a transitional zone between the arid Sahara (desert) to the north and the belt of humid savannas to the south. The climate of the Sahel is arid and hot, with strong seasonal variations in temperature and rainfall. The Sahel monthly mean temperatures vary from a maximum of 33°C to 36°C to a minimum of 18°C to 21°C (Buontempo et al. 2012a, 2012b; Ankidawa et al. 2018; Tomalka et al. 2021). During the winter, hot, dry Harmattan winds off the Sahara can bring sand and dust storms. The Sahel receives a yearly rainfall of about 200–600 mm, which falls mostly in the May to September monsoon season (Nicholson 2013; Basutti 2019). The rainfall is generally higher in the south, declining rapidly as one reaches the northern edge of the Sahel. However, the rainfall is characterised by great variation from year to year and from decade to decade. On interannual and decadal time scales, Sahelian rainfall is known to be affected by a variety of regional and global sea surface temperature (SST) anomaly patterns (Rowell 2003; Vizy and Cook 2001; Jung et al. 2006; Buontempo et al. 2012a, 2012b).

2.2 | Data

This study analysed monthly climate simulations, reanalysis and observational datasets. The simulation datasets consist of 25 historical GCM simulations from the Coupled Model Intercomparison Project, version 6 (CMIP6), downloaded from Earth System Grid Federation (ESGF) (https://esgf-node.llnl.

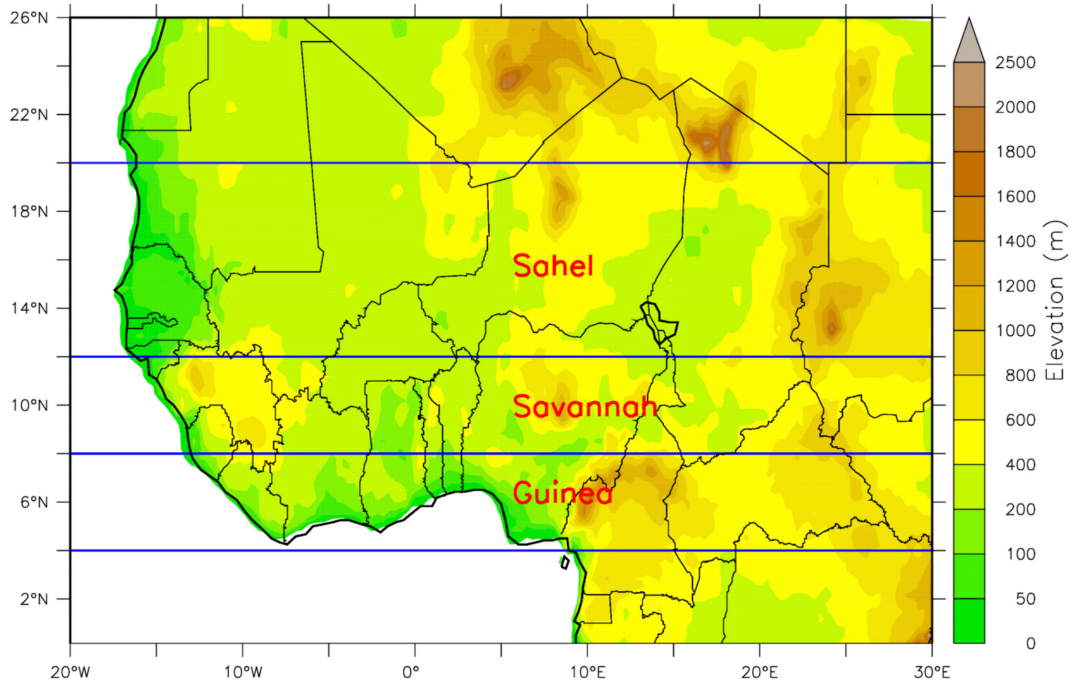

FIGURE 1 | West African domain showing the topography (in meters) and the climatic zones (Sahel, Savannah and Guinea) as used in the study. [Colour figure can be viewed at wileyonlinelibrary.com]

gov/search/cmip6/). These GCMs (Table 1) were chosen mainly based on the availability of the atmospheric variables needed for the study, whereas two coarse-resolution model (~250 km) was removed to avoid artificial spatial detail introduced during regridding. The variables used in the analysis are temperature, precipitation, wind (zonal and meridional components), vertical velocity, geopotential height and specific humidity. The reanalysis dataset is the fifth generation of the European Centre for Medium-Range Weather Forecast (ECMWF) Atmospheric Reanalysis (ERA5) obtained from the Copernicus Climate dataset website (https://cds.climate.copernicus.eu). It is the ECMWF's latest high-resolution (0.25°×0.25°) reanalysis dataset that combines vast amounts of historical observations into global estimates using advanced modelling and data assimilation systems. The ERA5 is globally complete and consistent in time (Hersbach et al. 2019).

In addition to ERA5, the Modern-Era Retrospective Analysis for Research and Applications, version 2 (MERRA-2, hereafter MERRA) obtained from the Goddard Earth Science Data and Information Services (https://disc.gsfc.nasa.gov/datasets), was included in the evaluation. MERRA is a global atmospheric reanalysis (with a horizontal resolution of 0.5°×0.625°) from the NASA Global Modelling and Assimilation Office (GMAO), which assimiliates space-based observations and includes updates from the Goddard Earth Observing System (GEOS) model. It provides an independent, well-validated representation of atmospheric circulation and moisture over Africa.

Furthermore, the Climate Forecast System Reanalysis (CFSR; 0.5°×0.5° grid resolution) obtained from the Geoscience Data Exchange (GDEX; https://gdex.ucar.edu/datasets/) was also used to assess inter-reanalysis uncertainty. Although CFSR shows broad consistency with ERA5 and MERRA in near-surface circulation metrics, it exhibits systematic structural differences in (i) the vertical extent of the West African Westerly Jet, (ii) jet-precipitation coupling over the Sahel and (iii) moisture transport intensity and pathway. Hence, CFSR is not used as a primary reference for the diagnostics but is included in the Supporting Information to document reanalysis-dependent sensitivities.

The observation dataset is the precipitation and near-surface temperature dataset from the Climate Research Unit (CRU) TS v4.03 (https://crudata.uea.ac.uk/cru/data/hrg/). The CRU dataset is a widely used climate dataset with a grid resolution of 0.5°×0.5° and provides monthly datasets dating back to 1901, covering all land domains of the world except Antarctica (Trenberth et al. 2013; Harris et al. 2020). CRU precipitation is used in preference to reanalysis precipitation because reanalysis rainfall is model-generated and subject to convective biases over West Africa (Maidment et al. 2013; Quagraine et al. 2020; Datti et al. 2024), whereas gauge-based datasets provide a more reliable representation of Sahel rainfall variability (Becker et al. 2013; Nicholson et al. 2018). The CRU, ERA5 and MERRA datasets were used to evaluate the GCM datasets over West Africa.

For the evaluation, all datasets, including observations, reanalysis and CMIP6 models, were regridded to a common grid of 0.5°×0.5° horizontal resolution using a bilinear interpolation method for comparability and analysed for a 35-year period (1980–2014). The target grid was chosen as a compromise resolution between the CMIP6 models (~100 km) and the reanalysis and observational datasets (ranging from 0.25° to 0.5° resolution). This is to avoid excessive upscaling while ensuring consistency across all datasets. We note that interpolating a coarser model field onto a finer grid does not create new small-scale information. Hence, diagnostic interpretation is therefore made at the scale of the observational/reanalysis products.

TABLE 1 | Simulations alias, model names and key reference of CMIP6 models used in this study. All simulations have approximately 100 km horizontal resolution.

Simulation	Model name	Variant	References
AWICM	AWI-CM-1-1-MR	r1i1p1f1	Semmler et al. (2018)
ECE-A	EC-Earth3	r1i1p1f2	EC-Earth (2019)
ECE-B	EC-Earth3-Veg	r1i1p1f3	EC-Earth-Veg (2019)
BCCCS	BCC-CSM2-MR	r1i1p1f4	Wu et al. (2018)
FGOAL	FGOALS-f3-L	r1i1p1f5	Yu (2019)
CAMSC	CAMS-CSM1-0	r1i1p1f6	Rong (2019)
FIOES	FIO-ESM-2-0	r1i1p1f7	Song et al. (2019)
CASES	CAS-ESM2-0	r1i1p1f8	Chai (2020)
GFDLC	GFDL-CM4	r1i1p1f9	Guo et al. (2018)
CES-A	CESM2	r1i1p1f10	Danabasoglu (2019b)
CES-B	CESM2-WACCM	r1i1p1f11	Danabasoglu (2019a)
CES-C	CESM2-WACCM-FV2	r1i1p1f12	Danabasoglu (2019a)
HADGE	HadGEM3-GC31-LL	r1i1p1f3	Ridley et al. (2019)
INM-A	INM-CM4-8	r1i1p1f1	Volodin et al. (2019a)
INM-B	INM-CM5-0	r1i1p1f2	Volodin et al. (2019b)
CIESM	CIESM	r1i1p1f3	Huang (2019)
CMCCC	CMCC-CM2-SR5	r1i1p1f4	Lovato and Peano (2020)
MPIES	MPI-ESM1-2-HR	r1i1p1f5	Jungclaus et al. (2019)
E3S-A	E3SM-1-0	r1i1p1f6	Bader et al. (2019a)
E3S-B	E3SM-1-1	r1i1p1f7	Bader et al. (2019b)
E3S-C	E3SM-1-1-ECA	r1i1p1f8	Bader et al. (2020)
MRIES	MRI-ESM2-0	r1i1p1f9	Yukimoto et al. (2019)
SAMUN	SAM0-UNICON	r1i1p1f10	Park and Shin (2019)
TAIES	TaiESM1	r1i1p1f11	Lee and Liang (2020)
NOESM	NorESM2-MM	r1i1p1f1	Seland et al. (2020)

2.3 | Method

Following previous studies (Pu and Cook 2010, 2012; Liu et al. 2020), we define the WAWJ as a low-level westerly jet over the eastern Atlantic and the West African coast. To identify the jet, we first select wind data for the domain 0° N—20° N and 40° W—10° W. From this domain, we select grid boxes where the zonal wind (u) is greater than or equal to 2 ms^{-1} and where the meridional wind (v) is greater than or equal to zero (0 ms^{-1}). The threshold of 2 ms^{-1} was determined based on the average core speed of the jet at stage 1 (the formation stage) as defined by Pu and Cook (2010) and as depicted by both the longitude-vertical and latitude-vertical profile of the zonal wind (not shown) using the reanalysis dataset (ERA5). All gridboxes which meet these criteria are included in the domain for the WAWJ. We also define the jet core area as a rectangular box measuring 7° of longitude by 2° of latitude. To locate this box, we find the peak wind speed (maximum u) at 925 hPa within the WAWJ domain. The box is centred on the peak wind speed unless doing so would extend it beyond the boundaries of the WAWJ region. In that case, the box is adjusted, manually, to both include the peak wind speed and fit within the WAWJ region. Although the size of the area remains consistent across all datasets (7° × 2°), the specific location of the jet core area varies among the datasets. We determined the WAWJ strength by computing the average value of the jet within the jet core area. Using these definitions of the WAWJ domain, the WAWJ jet core area and the WAWJ strength, we locate and compare the characteristics of WAWJ in ERA5 reanalysis and CMIP6 simulations over 35 years (1980–2014). The analysis focuses on the climatological structure and interannual variability of the jet as well as the relationship of the jet with other climate variables (precipitation and near-surface temperature) over West Africa. For ERA5 and the majority of CMIP6 simulations, the jet core is at 925 hPa and its maximum strength is in August. So, for most of the analyses reported in this paper, the 925 hPa was used as the default level, and August as the default month.

For the climatological structure, we consider the annual cycle and the vertical and horizontal structure of the jet. In the analysis of the annual cycle, we calculate the monthly climatology of the re-gridded datasets, locate the WAWJ domain and the jet core area, and extract the maximum speed (ms^{-1}) of the jet. In the vertical structure analysis, we calculate the August climatology of the zonal wind and vertical velocity. We average the fields along the latitude and the longitude to examine the longitude-vertical and latitude-vertical distributions of the jet respectively, averaged over the jet core area. For the horizontal structure analysis, we calculate the August climatology of the geopotential height and zonal and meridional wind at 925 hPa and locate the WAWJ domain and the jet core area. We also identify the ITCZ by selecting all grid boxes within 0° N—20° N and 40° W—10° W where meridional wind is zero (0 ms^{-1}), consistent with previous studies that characterise the ITCZ as the latitude of meridional wind reversal (Thorncroft and Blackburn 1999; Žagar et al. 2011; Nicholson 2018). The capability of the CMIP6 simulations to reproduce the spatial pattern in the reanalysis was quantified with spatial correlation and percentage bias. The percentage bias (PBIAS) was calculated as follows:

$$\mathrm{PBIAS} = \frac{\overline{X_s} - \overline{X_o}}{\overline{X_o}} \times 100 \quad (1)$$

where $\underline{X_s}$ is the spatial average of the simulated values. $\underline{X_o}$ is the spatial average of the reanalysis values.

For each dataset, we compare the interannual variability of WAWJ and Sahel precipitation. It is important to note that CMIP6 simulations are uninitialised and therefore we would not expect them to simulate the year-to-year evolution of climate variability in the same way as has been observed in reality. Our analysis does not directly compare time series from models with observations or reanalysis. Instead, it focuses on quantifying the magnitude of interannual variability and the interannual relationship between the WAWJ and precipitation. The interannual variability of the WAWJ is represented using the August anomalies of the WAWJ strength (at 925 hPa), calculated for each year relative to the long-term August climatological mean. The interannual variability of Sahel precipitation is calculated as standardised precipitation anomalies. That is, we calculate the August precipitation anomalies for each year relative to the long-term August climatological mean over the Sahel (averaged over 18° W–30° E, 10° N–20° N), and normalise them by the standard deviation. This slightly differs from the Sahel domain defined in the study area (12° N –20° N, 20° W–20° E), which was used only to delineate subregions for descriptive purposes. The adjustment ensures that averaging and interannual variability calculations are not biased by oceanic or marginal grid points. The characteristics of the WAWJ strength time series are quantified with the linear trend and standard deviation while the relationship between the WAWJ and precipitation time series is quantified with Pearson's correlation coefficient. The significance of the trendline (gradient) and correlation coefficient is calculated using Student's *t*-test at a 95% confidence level.

To examine the relationship between the WAWJ and the spatial distribution of climate variables (i.e., temperature and precipitation) over West Africa, we perform a temporal correlation between the WAWJ strength time series and the time series of each climate variable at each grid point over West Africa in August at 925 hPa (1980–2014). The spatial distribution of the correlation coefficient obtained for each CMIP6 simulation dataset is compared with the one obtained for the ERA5 dataset. The comparison is quantified with spatial correlation analysis and a significance test (Student's *t*-test) at a 95% confidence level. We also examine composites of WAWJ positive and negative modes, by selecting the 3 years with the highest and 3 years with the lowest WAWJ strength anomalies relative to the August climatological mean. We examine the spatial distribution of precipitation, temperature and moisture flux associated with these composites. Lastly, we compare the absolute error in the simulated precipitation and the WAWJ-Sahel precipitation link. The absolute error was calculated by subtracting the mean of the simulated from the mean of the observed precipitation in the Sahel and the WAWJ-Sahel precipitation link is represented with the correlation value between WAWJ-strength and Sahel precipitation.

3 | Results and Discussion

This section will describe and discuss the analysis of the annual cycle of the WAWJ, its horizontal and vertical structure, interannual variability and the relationship with temperature and rainfall.

3.1 | Annual Cycle of the WAWJ

The annual cycle of the WAWJ exhibits a broadly consistent seasonal structure across the three reanalysis products (ERA5, MERRA and CFSR) as reported in Pu and Cook (2010, hereafter PC2010), including the five-stage evolution of the jet. However, important differences emerge in the timing of onset, intensification and peak season. Among the three datasets, ERA5 provides the most realistic representation, capturing both the expected June onset and the canonical five-stage evolution of the jet (Figure 2).

ERA5 and MERRA show very similar seasonal evolution and jet intensity. In both datasets, the jet emerges in June with a core speed of about 2.1 ms^{-1} (ERA5) and 2.3 ms^{-1} (MERRA) in Stage 1. It then intensifies steeply as the jet's core speed increases through June–July, reaching 4.1 ms^{-1} (ERA5) and 4.8 ms^{-1} (MERRA) in Stage 2. The jet attains its peak strength of about 5.3 ms^{-1} (ERA5) and 5.5 ms^{-1} (MERRA) in Stage 3 (August) and weakens as its core speed reduces to about 2.9 ms^{-1} (ERA5) and 3.5 ms^{-1} (MERRA) in Stage 4 (September). However, it is difficult to distinguish between Stage 4 (the weakening stage) and Stage 5 (the dissipating stage; $< 2\,ms^{-1}$) of the jet in a monthly dataset. Pu and Cook (2010) found that Stage 4 of the jet occurs between the 6th and 19th of September, whereas Stage 5 occurs between the 20th and 18th of October. This distinction can only be illustrated in a daily dataset. Despite the differences in the temporal resolution of the data used in PC2010 (i.e., daily) and the present study (i.e., monthly), the strength of the jet obtained here agrees with those reported in PC2010 at each stage. This implies that the main characteristics of the annual cycle of the jet can be described with monthly datasets.

In contrast, CFSR displays a markedly different evolution of the WAWJ among the three reanalysis products. For instance, CFSR exhibits an anomalously early onset, with the jet strengthening rapidly between January and April, reaching a premature peak of 5.8 ms^{-1} in April well before the main monsoon season. Thereafter, the jet weakens through May–June down to about 4.2 ms^{-1}, followed by a modest secondary peak of about 5.4 ms^{-1} in August before declining to 3.6 ms^{-1} in September. This early-spring maximum and mid-summer weakening in CFSR is consistent with previously documented structural biases between reanalysis products over West Africa, including disagreements in low-level moisture and precipitation timing and highlights known limitations of older reanalysis systems in representing pre-monsoon circulation and convective timing (Roberts et al. 2015; Robertson et al. 2016; Quagraine et al. 2020). For completeness, we further examine CFSR (briefly) and reveal a systematically shallower vertical structure of the WAWJ compared to ERA5 and MERRA (Appendix S1, Appendix S2, Figures A1.1 and A1.2), weaker relationship in the jet-precipitation coupling over West Africa (Appendix S1, Figures A1.3 and A1.4) and moisture transport intensity (Appendix S1, Figure A1.5) compared to ERA5 and MERRA. Hence, we do not include CFSR in subsequent analysis beyond this point but focus on ERA5

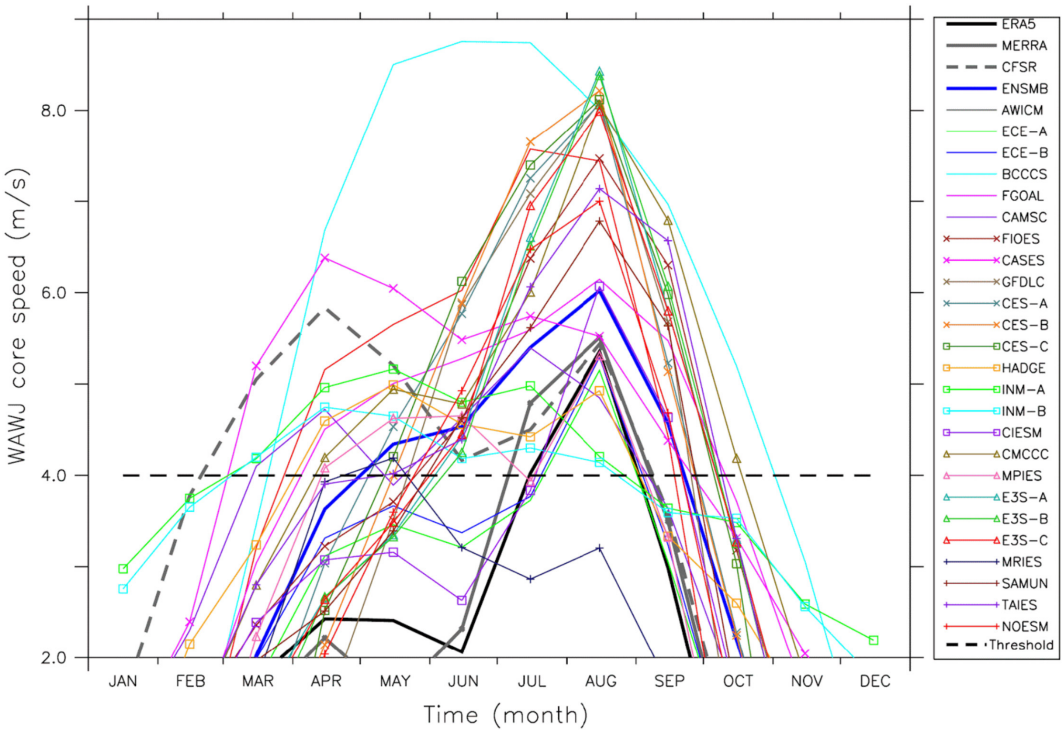

FIGURE 2 | The magnitude and annual cycle of WAWJ core strength climatology from 1980 to 2014 at 925 hPa as observed in ERA5 (thick solid black), MERRA (solid grey), CFSR (dashed grey) and simulated by CMIP6 models and the ensemble mean (ENSMB). The black dashed line shows 4 ms^{-1}, which indicates the average speed of the jet at maturity (stage 2), to aid comparison with models. The blue dashed line is the model's ensemble mean. [Colour figure can be viewed at wileyonlinelibrary.com]

and MERRA, which exhibit consistent annual cycle, realistic onset timing and broadly comparable structure, providing a robust foundation for the evaluation.

The majority of the CMIP6 simulations depict the key features of the summer cycle of the jet, with intensification in June to July, peak in August, followed by weakening (Figure 2). However, there are notable biases in the model results. Firstly, the jet develops too early in many models. For example, the jet already attains Stage 3 (speed $\geq$4.0) in February in 5 models (20%), March in 7 models (28%), April in 8 models (32%), and May in 2 models (8%). Only 3 models (ECE-A&B and CIESM) simulate Stage 3 in August, as depicted in ERA5 and MERRA results. It is important to note that the difference between the stages can be distinguished not only as a function of peak speed but also as a function of how the speed changes as each stage progresses. Some models show a direct intensification from the start to the maximum speed in August without distinguishable intermediate stages. In other words, even if these models peak in August, they do not accurately represent Stage 3, which requires a clear progression from earlier stages. Secondly, the jet is too strong in most models. The peak strength of the jet is more than 5 ms^{-1} in 14 models (56%) and even more than 8 ms^{-1} in 8 models (32%). Thirdly, the weakening of the jet (Stage 4; speed $<4.0\,m^{-1}s$) is also prolonged in most models. Only 5 models (19%) simulate weakening to $<4.0\,m^{-1}s$ in September, 12 models (48%) simulate it in October while 2 (8%) feature it in November. These model biases are illustrated in the ensemble mean, which features a jet that develops too early, that is the jet already attains stage 2 in April and overestimates the jet speed at all stages of the jet ($>3.6\,ms^{-1}$ in stage 1; $>5.4\,ms^{-1}$ in stage 2 and $>6.0\,ms^{-1}$ in stage 3). There are also 4 models (CASE, HADGE, INM-A&B and MRIES) which fail to simulate the structure of the annual cycle of the jet. For instance, in MRIES, the jet features in March (speed = 2.4 ms^{-1}), intensifies steeply and reaches maximum speed (4.5 ms^{-1}) in April, persists till May, weakens in July and disappears in August.

3.2 | Horizontal Structure of the WAWJ

ERA5 and MERRA both capture the (and show very similar) spatial structure of the WAWJ in August as in PC2010 (Figure 3). In ERA5, the WAWJ, which is located off the coast of West Africa, extends from 6° N to 12° N and from 5° W to 35° W and the jet core is located around 8° N and 20° W. The jet is associated with an offshore extension of the thermal low, as indicated by the trough (i.e., 780-gpm contour, shown as a blue contour line in Figure 3) extending from over the continent to around 30°W over the ocean. MERRA reproduces the same large-scale pattern, the westward extension of the thermal low and positions the WAWJ in a similar latitudinal band as in ERA5. However, important differences emerge in the structure of the thermal low and the horizontal extent of the jet. Compared with ERA5, MERRA shows a shallower westward extension of the thermal low (indicated with the 905-gpm contour in Figure 3). Instead of the 780-gpm contour as in ERA5, MERRA exhibits a westward extension of the 905-gpm contour, which only reaches approximately 27° W. This weaker westward penetration of the trough could be associated with the horizontally contracted jet structure (and its core) in MERRA (Figure 3) and the slight underestimates of the jet strength (indicated by the PBIAS = −6%).

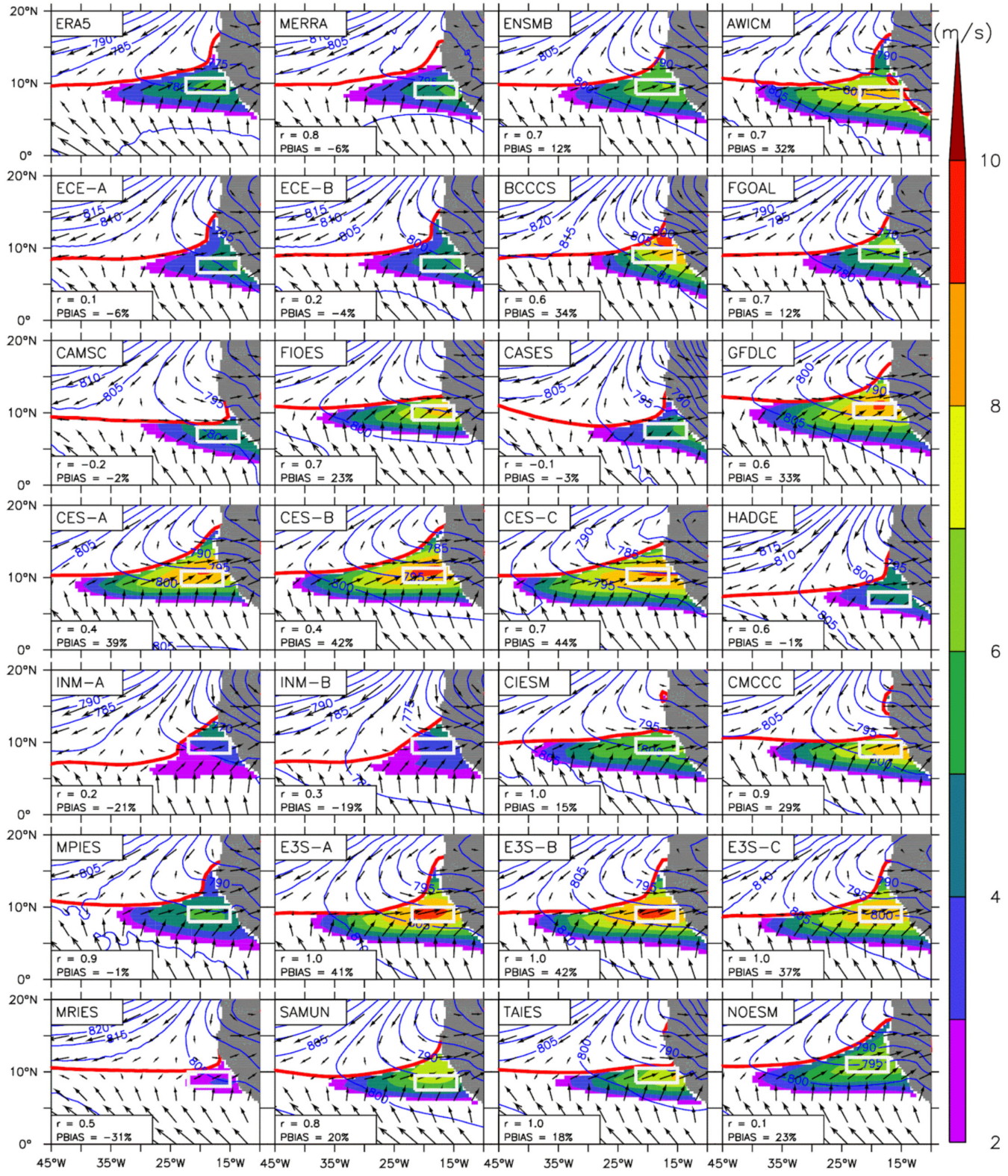

FIGURE 3 | The spatial distribution of WAWJ climatology (1980–2014) and the associated ITCZ (red line; defined as a line where the meridional wind is zero (i.e., $v=0$)), geopotential heights (blue contours; gpm) and wind patterns (black vectors) in August at 925 hPa, for ERA5, MERRA and CMIP6 models. The shaded region indicates the WAWJ domain and the zonal wind speeds (ms^{-1}) within it. The white box indicates the area designated as the WAWJ core area. The spatial correlation coefficient and the percentage bias are shown for each model in the bottom right of the panel. [Colour figure can be viewed at wileyonlinelibrary.com]

Despite these differences, the agreement between MERRA and ERA5 is high. The spatial correlation ($r=0.7$) demonstrates strong coherence in the placement and shape of the jet.

Most CMIP6 models, including the multi-model ensemble mean, produce a westerly jet off the coast of West Africa but the capability of the models to replicate the spatial structure varies,

as depicted by the spatial correlation (r) of the simulated structure with the reanalysis and by the associated simulation bias (i.e., PBIAS; percentage bias), indicated in the bottom left panels of Figure 3. Although 12 models (48%) feature a strong to very strong positive correlation ($r \geq 0.7$) with the ERA5 reanalysis, 6 models (24%) have a moderate positive correlation ($0.4 \leq r \leq 0.6$), 5 models (20%) shows a weak positive correlation ($0.1 \leq r \leq 0.3$) and 2 models (8%) show negative correlation ($-0.3 \leq r \leq 0$) with the ERA5 reanalysis.

When evaluated against ERA5, the latitude of the jet core varies between models (as indicated by the white boxes in Figure 3), with some models placing the jet core too far south (CAMSC, CASES). Most models overestimate area coverage and the core strength of the jet. Their PBIAS ranges from 12% (in FGOAL) to 44% (in CES-C). For example, in CES-C (which shows the highest PBIAS), the jet stretches from 5° N—14° N and 15° W—40° W with a core strength of more than 8 ms^{-1}. Only 9 models (ECE-A & B, CAMSC, CASES, HADGE, INM-A & B, MPIES and MRIES) feature negative PBIAS (−31% to −1%). In MRIES (that have the largest negative bias) the jet only stretches from 7° N—11° N and 15° W—23° W with a core strength of less than 4 ms^{-1}. Nevertheless, the ensemble mean produces a jet pattern with a strong correlation ($r \geq 0.7$) and similar area coverage to the observed but slightly overestimated the core strength (about 6 ms^{-1}).

The differences between models in the horizontal structure of the WAWJ are associated with differences in the ITCZ, and the geopotential height and wind fields. These imply differences in the strength and location of the Saharan Heat Low, as found in previous studies (e.g., Annor et al. 2023; Dixon et al. 2017).

3.3 | Vertical Structure of the WAWJ

The latitude-height cross-section of the zonal wind along the jet's longitudes in August is shown in Figure 4, with each panel for ERA5, MERRA and the CMIP6 models illustrating how the jet deepens and extends from South (on the left-hand side) to North (on the right-hand side). In both ERA5 and MERRA, the jet extends from the surface to about 750 hPa, but the core of the jet (about 4 ms^{-1}) is at 925 hPa. This is consistent with PC2010 results. The African Easterly Jet (AEJ) core is located above (600 hPa) and north (centred on 16ºN) of the WAWJ (shown by the dotted contours) in both reanalysis products. This agrees with the finding of Grist and Nicholson (2001) that equatorial westerlies (including WAWJ) displace the AEJ (and its associated disturbances) northward and modulate the interannual variability of AEJ. Their study also found that the northward displacement of AEJ coincides with wet years in the Sahel because it enhances both the horizontal and vertical wind shear over the Sahel.

Most of the CMIP6 models and the ensemble mean capture the vertical structure of the jet as in the ERA5 reanalysis and show the AEJ to the north of the WAWJ. This coincides with the June–August wet season over the Sahel when the AEJ is known to shift northward (Bercos-Hickey and Patricola 2021). However, the models show different capabilities in simulating the vertical extent of WAWJ, the latitude of the WAWJ core and the associated northward location of AEJ. The jet extends to 750 hPa (or above) in only 14 models (56%) and to 800 hPa in 7 models (28%) and the ensemble mean. One model (MRIES, which simulates the weakest WAWJ) features the jet below 900 hPa and puts the jet core at 1000 hPa. Some models simulate too much vertical extension of the WAWJ (e.g., AWICM). The latitude of the jet core also varies between models; for example, it is particularly far north (up to 11° N or 12° N) in CES-B.

The structure of the WAWJ appears to be related to the AEJ. Those models that show a more extensive WAWJ tend to have a more northward AEJ (e.g., AWICM, CES-B, E3S-A), whereas those with a weak WAWJ which is confined in the lower layers of the atmosphere appear to have a southward shifted AEJ (e., HADGE, INM-A & B, MPIES). Previous literature has illustrated variation between CMIP models in the latitude of the AEJ (Kuete et al. 2022). This also relates to upward motion, illustrated by vertical vectors in Figure 4. As illustrated in ERA5 and MERRA, there is pronounced upward motion through the depth of the troposphere between approximately 8° N. and 12° N. As Figure 4 shows, this corresponds to the latitude of the WAWJ. Those models with a northward WAWJ also show the vertical motion further north (e., CES-B, FIOES).

The longitude-height cross-section of the zonal wind speed along the jet's latitudes in August is shown in Figure 5. The figure shows the jet core (4 ms^{-1}) between 25° W and 15° W in the ERA5 and between 22° W and 10° W in MERRA, which is both 2 ms^{-1} weaker and extends more westward than in PC2010. This small discrepancy could be because our study uses averaged values over 8° N–10° N, whereas PC2010 used values along a single latitude (9.5° N). Some of the models capture the vertical structure of the jet in the longitudinal cross-section. However, most of the models fail to clearly distinguish the WAWJ. For instance, the CES-C model features the westerly flow maxima from about 28° W to 12° E without any distinction. The INM-A model failed to capture the WAWJ and only features a westerly flow maximum at 10° E.

3.4 | Inter-Annual Variability of the WAWJ

Since the CMIP6 models are uninitialized, we would not expect them to follow the same interannual evolution of climate as has occurred in reality. Therefore, we cannot evaluate interannual variability by directly comparing the time series. Instead, we have calculated statistics to quantify the magnitude of interannual variability (standard deviation) and the linear trend, as well as the correlation between the WAWJ and Sahel precipitation in each dataset. The capability of CMIP6 simulations to reproduce the interannual variability of WAWJ, as in the reanalysis (ERA5 and MERRA) and CRU precipitation, differs (Table 2). ERA5 shows a strong positive trend (tr = 0.04 ms^{-1} $years^{-1}$) in the interannual variability of the jet strength. This positive trend is related to the partial recovery of precipitation in the Sahel, which began in the 1990s (Hagos and Cook 2008; Pu and Cook 2010, 2012). The trend (1.402 mm $month^{-1}$ $years^{-1}$) in Sahelian precipitation in ERA5 is an indication of the significant recovery in rainfall. Though MERRA captures the positive trend in both WAWJ interannual variability and the subsequent Sahelian precipitation, supporting the broader narrative of regional

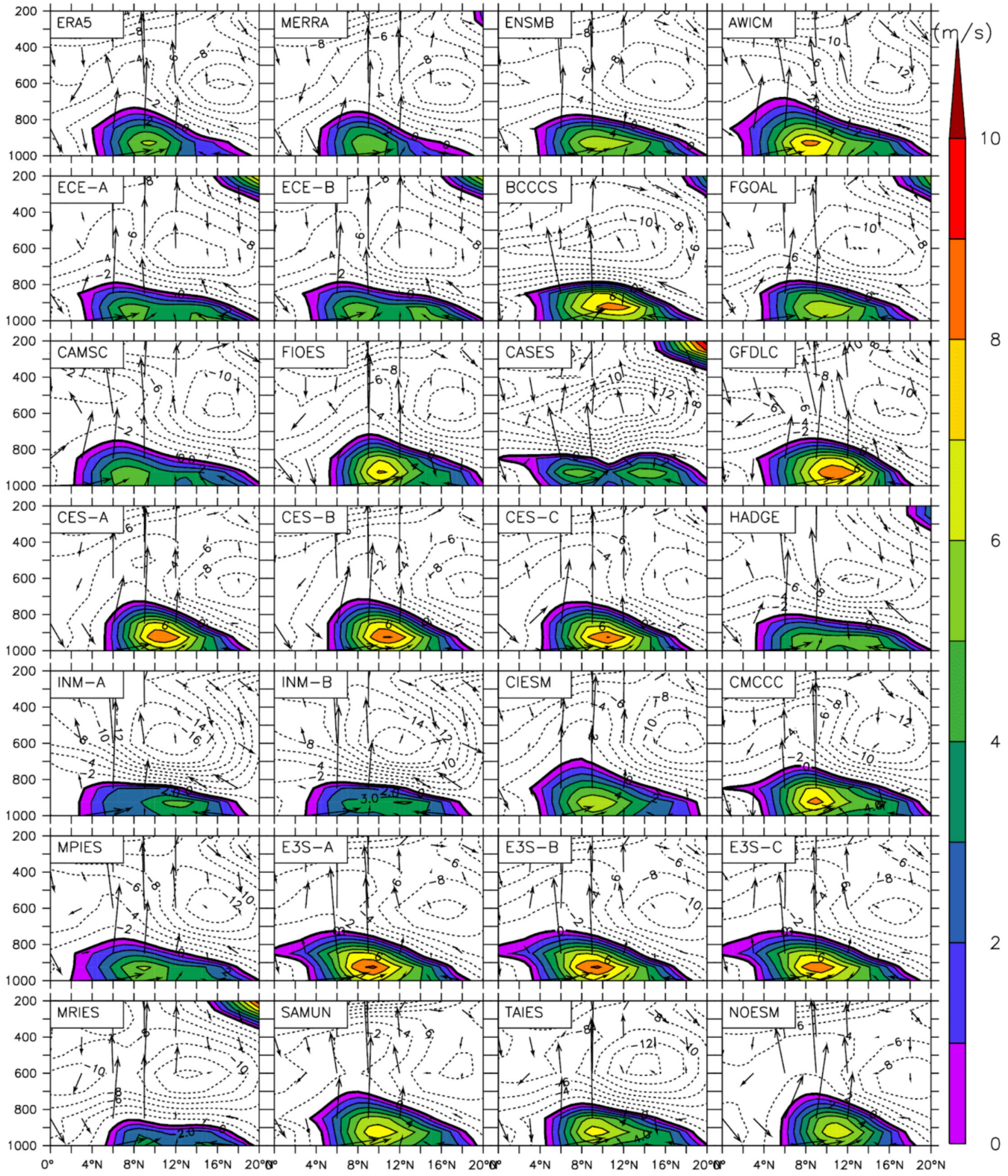

FIGURE 4 | Cross-sections of August zonal wind speed (ms^{-1}; contours—dotted contours are easterlies; westerlies shaded) averaged along the (7°) longitude of the jet core area (white boxes in Figure 3—different for each model), with vectors of meridional and vertical winds (multiplied by 10^2), for ERA5, MERRA and CMIP6 models and its ensemble. [Colour figure can be viewed at wileyonlinelibrary.com]

hydroclimatic recovery. However, these trends are substantially weaker in magnitude ($tr = 0.000002219\,ms^{-1}\,years^{-1}$ for the jet; $tr = 0.00003201\,mm\,month^{-1}\,years^{-1}$ for precipitation), suggesting that MERRA represents a more muted intensification. This may reflect known limitations of the dataset in representing long-term moisture balance and precipitation over West Africa (e.g., moisture-budget imbalances; Quagraine et al. 2020).

The majority of the models, including the ensemble mean, capture the positive trend of the jet ranging from

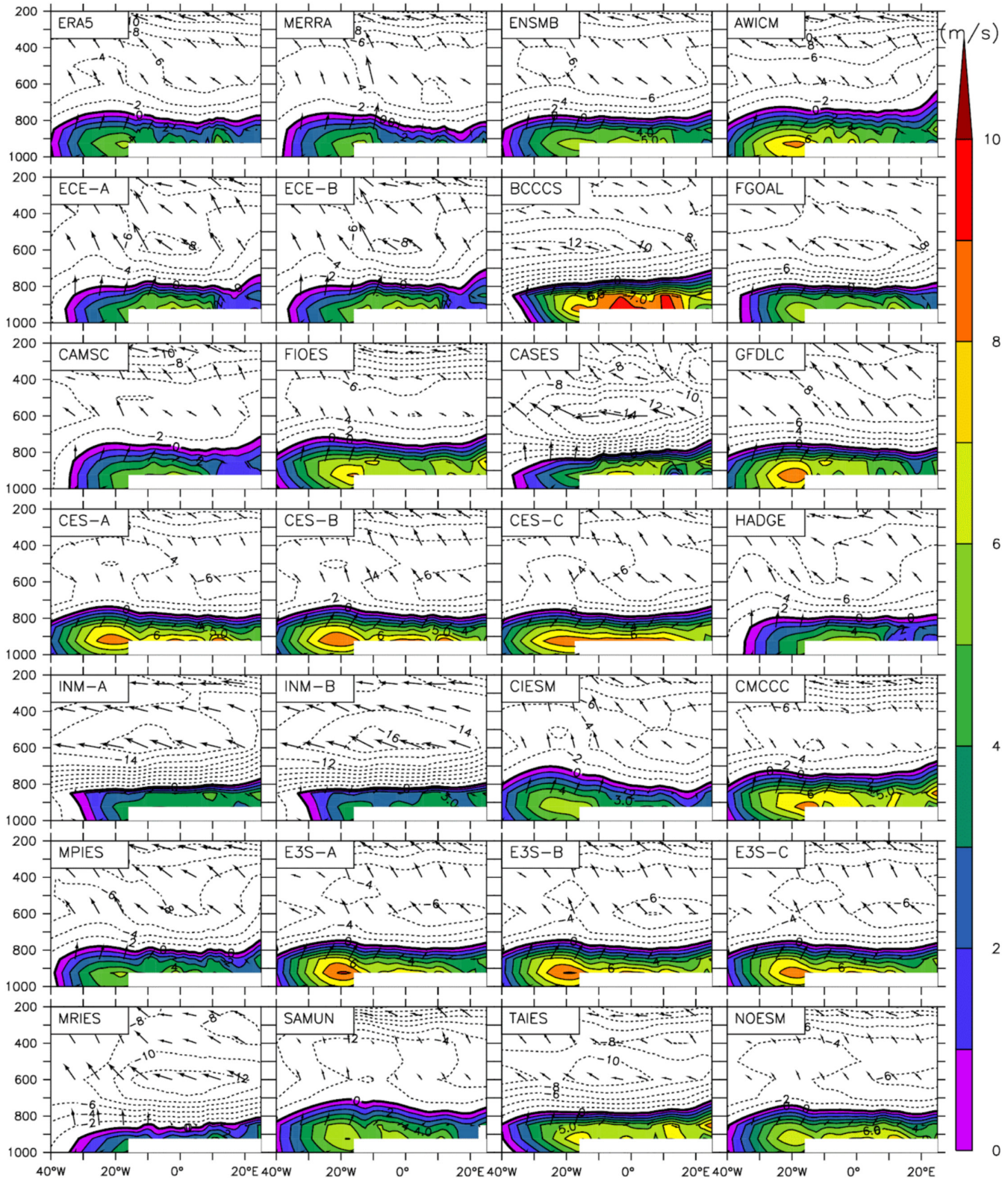

FIGURE 5 | Cross-sections of August zonal wind speed (ms^{-1}; contour—dotted contours are easterlies; westerlies shaded) averaged along the (2°) latitude of the jet core area (white boxes in Figure 3—different for each model), with vectors of zonal and vertical winds (multiplied by 10^2). [Colour figure can be viewed at wileyonlinelibrary.com]

0.002 ms^{-1} $years^{-1}$ (in FGOAL) to 0.05 ms^{-1} $years^{-1}$ (in ECE-A and CES-B). For these models, the corresponding trends in Sahel precipitation range from 0.09 mm $month^{-1}$ $years^{-1}$ (in FGOAL) to 1.188 mm $month^{-1}$ $years^{-1}$ (in ECE-A). However, 3 models (CAMSC, E3S-A, E3S-C) show a negative trend (tr ≤ -0.017 ms^{-1} $years^{-1}$) in the interannual variability of the jet strength. For these models, the trends in Sahel precipitation are -0.111 mm mon^{-1} $years^{-1}$ (CAMSC), 0.6786 mm mon^{-1} $years^{-1}$

TABLE 2 | The statistical summaries of WAWJ strength (ms^{-1}; averaged over the jet core area), along with the precipitation time series (PPT) over the Sahel region (10° N–20° N, 18° W–30° E) for August.

	Mean		Standard deviation		Trend		
Model	**WAWJ (ms^{-1})**	**PPT ($mm\,mon^{-1}$)**	**WAWJ (ms^{-1})**	**PPT ($mm\,mon^{-1}$)**	**WAWJ ($ms^{-1}\,years^{-1}$)**	**PPT ($mm\,mon^{-1}\,years^{-1}$)**	**Correlation**
ERA5 (CRU)	5.07	135.40	1.14	26.59	0.0465*	1.402*	0.8*
MERRA (CRU)	5.23	135.4	1.60	26.59	2.22E-06*	3.20E-05*	0.74*
ENSMB	5.79	89.07	0.26	6.12	0.0159*	0.4944*	0.79*
AWICM	7.18	120.70	0.89	23.14	0.0131	0.5049	0.6*
ECE-A	4.40	65.36	0.90	18.70	0.0506*	1.188*	0.8*
ECE-B	4.61	72.29	0.68	14.88	0.0263*	0.7455*	0.8*
BCCCS	6.74	72.02	0.55	15.79	0.0157	0.0355	0.4*
FGOAL	5.69	38.05	0.92	14.61	0.0016	0.0944	0.4*
CAMSC	4.58	78.46	0.99	14.99	−0.0172	−0.111	0.2
FIOES	6.88	146.10	0.75	14.65	0.0060	0.1996	0.6*
CASES	4.61	48.66	0.46	18.81	0.0103	0.7664*	0.3
GFDLC	7.66	131.10	0.89	29.55	0.0212	1.0430*	0.7*
CES-A	7.53	126.30	1.01	23.28	0.0251	0.7110	0.6*
CES-B	7.85	130.00	1.30	23.83	0.0496*	1.0940*	0.7*
CES-C	7.79	99.42	1.50	20.33	0.0305	0.9022*	0.6*
HADGE	4.17	67.32	0.76	15.42	0.0133	0.6469*	0.2
INM-A	3.38	66.68	0.42	16.93	0.0104	−0.0216	0.1
INM-B	3.44	63.94	0.62	15.62	0.0127	0.3793	0.4*
CIESM	5.75	0.14	1.26	0.022	0.0165	3.43E-04	0.9*
CMCCC	7.15	121.00	1.18	20.52	0.0472*	0.9351*	0.8*
MPIES	5.04	105.80	0.62	21.75	0.0217*	−0.0037	0.6*
E3S-A	7.98	120.40	1.34	19.08	−0.0180	0.6786*	0.3*
E3S-B	7.96	110.90	1.53	20.96	0.0350	0.5895	0.7*
E3S-C	7.62	111.40	1.49	20.08	−0.0303	−0.1584	0.4*
MRIES	2.70	72.27	0.82	11.23	0.0239	0.2332	0.4*
SAMUN	5.85	159.10	1.15	25.75	0.0039	1.0260*	0.1
TAIES	6.40	97.11	0.88	22.48	0.0083	0.5615	0.7*
NOESM	6.61	137.6	1.02	20.73	0.0132	0.2866	0.7*

Note: For the observation, CRU precipitation was used alongside WAWJ strength from ERA5 and MERRA. The trend and the correlation were calculated for WAWJ anomalies and the standardised precipitation anomalies. The anomalies are calculated relative to the August climatological mean. The asterisk (*) symbol indicates statistical significance at the 95th percent confidence level.

(E3S-A) and $-0.1584\,mm\,mon^{-1}\,years^{-1}$ (E3S-C). The jet in these models also shows a weak positive correlation with precipitation over West Africa, particularly over the Sahel. This suggests that as the WAWJ strengthens over time, it enhances precipitation over West Africa, specifically over the Sahel. The standard deviation of the simulated WAWJ variability varies from 0.42 (in INM-A) to 1.5 (CES-C, E3S-B & C), with 16 models (64%) underestimating the variability. In ERA5, the interannual variability of the WAWJ is strongly correlated with Sahelian rainfall ($r = 0.8$). Comparing each CMIP6 model's correlation map with the ERA5 reference using spatial correlation coefficients reveals that 14 models (56%) show good agreement with ERA5, with a spatial correlation $r > 0.5$, whereas the remaining 11 models (44%) show weaker agreement. Across all models, the spatial correlation with ERA5 ranges from 0.11 (in INM-A, which also exhibits the lowest interannual variability of the WAWJ) to 0.8 (in CIESM). The multi-model ensemble mean reproduces the positive trend of the jet ($tr \geq 0.0167\,m\,s^{-1}\,years^{-1}$)

and shows a strong spatial agreement with ERA5 ($r > 0.8$), but underestimates the interannual variability of the jet, with a standard deviation of 0.26 m s^{-1}.

3.5 | WAWJ and the Spatial Distribution of Precipitation and Temperature Over West Africa

The previous section illustrated that many of the models are able to capture a positive correlation between the WAWJ and Sahelian precipitation when averaged over the Sahelian domain. We now investigate the spatial pattern of precipitation and temperature associated with the WAWJ strength. Observations and reanalysis (ERA5 and MERRA combined with CRU) show that there is a strong relationship between WAWJ strength and the spatial distribution of precipitation and temperature in West Africa (Figures 6 and 7). In both reanalyses, the jet features a strong correlation ($r > 0.6$) with precipitation over the Savanna and Sahel zones (10° N—30° N and 20° W—25° E; Figure 6). The peak correlation ($r \approx 0.8$) obtained in this study is even higher than those reported in Pu and Cook (2012, hereafter PC2012; $r \approx 0.6$). The jet also has a strong dipole correlation with the surface temperature (Figure 7), featuring a positive correlation ($r \approx 0.6$) north of 20° N but a negative correlation ($r \approx -0.7$) between 8° N—20° N in ERA5 (with CRU). Although the positive correlation can be attributed to the role of the Saharan heat-low in the formation of WAWJ (as discussed by PC2012 and implied by Figure 3), the negative correlation (between 8° N and 20° N in ERA5) is likely due to the influence of the jet on the temperature field through precipitation. Hence, the ERA5 (with CRU) results suggest that the stronger the intensity of the Saharan heat-low (i.e., the higher the temperature north of 20°N), the stronger the WAWJ (due to the associated stronger pressure gradient force between the continent and the Atlantic Ocean). MERRA (with CRU) reproduces the same correlation pattern between the jet and precipitation over the Savannah and Sahel region with a strong agreement ($r = 0.9$) with ERA5. In addition, MERRA exhibit a similar dipole structure in the correlation of WAWAJ with near surface temperature, although the southern limit of the negative-correlation band, in near-surface temperature, is shifted northward (approximately 12° N–20° N rather than 8° N–20° N in ERA5). This latitudinal shift may be attributed to the structural bias identified earlier in MERRA, particularly the weaker and less westward-extending Saharan heat-low signature and its slightly shorter jet core, which, together, could shift the region of strongest WAWJ-related hydroclimate anomalies northward.

To further explore this, we compute composites of the 3 strongest and 3 weakest August WAWJs and illustrate the anomaly between the positive and negative WAWJ modes in precipitation, temperature and moisture flux, in Figure 8. In the reference datasets (ERA5 and MERRA combined with CRU), the stronger WAWJ transports more moisture eastward into the continent within the 5° N—10° N band (Figure 8). Figure 8 shows enhanced transport of moisture from the tropical Atlantic band (5° N–10° N) into the Sahel (10° N–20° N) during strong WAWJ events. The WAWJ accelerates eastward winds over the Gulf of Guinea and the western Sahel, which carry moisture north-eastward into the continent. This enhanced moisture flux feeds into the low-level monsoon flow, reinforcing north-eastward moisture transport into the Sahel. As a result, precipitation and soil moisture increase over the region (not shown), leading to lower near-surface temperatures within 8° N–20° N (Figure 7). These results illustrate how variability in the WAWJ strength directly modulates the spatial distribution of moisture and associated hydroclimatic conditions across West Africa. These results are in agreement with previous studies (i.e., PC2012) that linked the yearly variation in WAWJ strength to interannual variability of precipitation in the Sahel.

Not all the CMIP6 models capture the relationship between the jet and the spatial distribution of precipitation and temperature as depicted in the reanalyses (Figures 6 and 7). Although most models reproduce the observed strong correlation between the jet and the climate variables, the pattern and magnitude of the correlation differ from those ERA5 and MERRA. For instance, in the relationship between the jet and precipitation (Figure 6), only 8 models (32%) feature a comparable pattern ($r \geq 5$; shown at the bottom left corner of Figure 6) with the map of ERA5, namely: ECE-A ($r = 0.5$), ECE-B ($r = 0.5$), GFDLC ($r = 0.5$), CES-B ($r = 0.5$), CIESM ($r = 0.6$), MPIES ($r = 0.5$), MRIES ($r = 0.5$) and TAIES ($r = 0.5$). All these models (except TAIES) and the ensemble mean agree with ERA5 that the positive phase of WAWJ produces a stronger eastward transport of moisture within the 8° N—20° N band from the west coast (≈20° W) up to 25° E. This moisture is then transported north-eastward to north of 20° N, leading to higher precipitation over the sub-continent north of 8° N (Figure 8). However, these models exhibit a weaker north-eastward transport of moisture compared to ERA5, indicating that the coupling between the WAWJ-driven eastward moisture transport and the monsoon-related north-eastward transport is underestimated. (Aadhar and Mishra 2020; Hourdin et al. 2015a, 2015b; Li et al. 2021; Stouffer et al. 2017). That may explain why the increase in precipitation during the stronger WAWJ is limited to south of 15° N in these models (Figure 8).

The remaining models (68%) have a weak agreement with ERA5 on the relationship between WAWJ and the spatial distribution of precipitation (Figure 6); their correlation with ERA5 ranges from 0.1 (INM-A and E3S-A) to 0.4 (FIOES, CMCC and NOESM). Although some of these models (e.g., AWICM, CASES and MPIES) capture the two distinct increases in moisture transports (i.e., the eastward and north-eastward transports) during stronger WAWJ, the moisture increase does not translate to a commensurable increase in precipitation north of 10° N as in ERA5. This behaviour is consistent with the process-based interpretation of Nicholson (2013), who argues that Sahel rainfall is only weakly sensitive to moisture availability once a baseline threshold is met. Beyond this threshold, rainfall becomes strongly controlled by dynamical factors such as low-level convergence, mid-tropospheric ascent and the initiation and organisation of mesoscale convective systems (MCSs). In the absence of adequate dynamical support, excess moisture alone is insufficient to trigger deep convection or sustain large-scale rainfall. Thus, for CMIP6 models that do not realistically simulate the dynamical environment of the monsoon system, increases in WAWJ-related moisture transport are unlikely to translate into increased precipitation, even when the moisture signal itself appears reasonable.

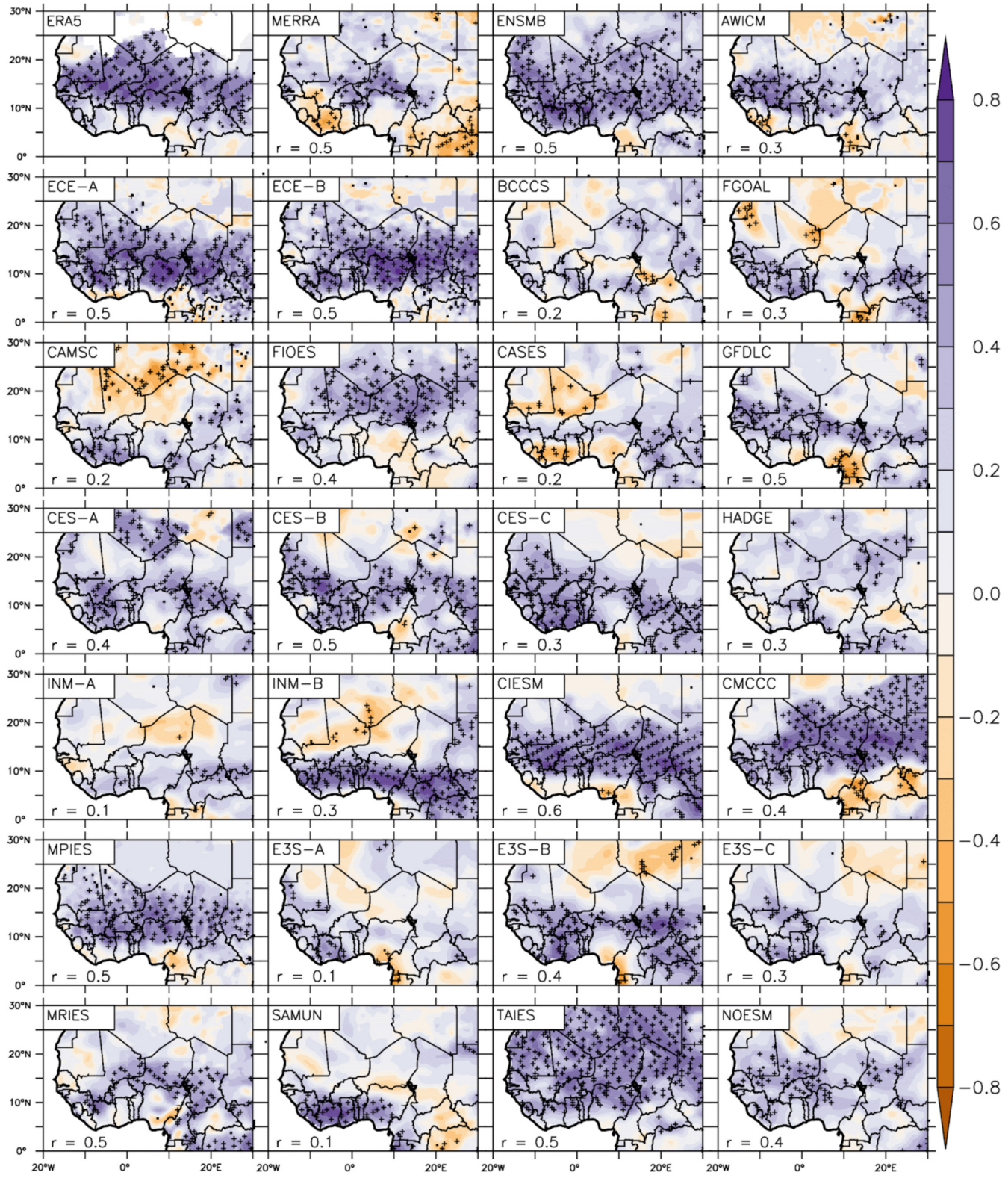

FIGURE 6 | The spatial distribution of correlation between time series of the WAWJ strength ($m\,s^{-1}$; averaged over the white boxes showing the jet core area in Figure 3) and precipitation (mm/month) over West Africa in August (1980–2014), as observed by ERA5 (WAWJ) and MERRA (WAWJ) with CRU (precipitation) and simulated by the CMIP6 models and the multi-model ensemble mean. The similarity between the simulated and observed patterns is quantified and indicated by a spatial correlation value in each panel, and significance at each grid point at a 95% confidence level is marked by a (+) symbol. [Colour figure can be viewed at wileyonlinelibrary.com]

However, some models fail to simulate the two distinct increases in moisture transports. With the increase in WAWJ, some models (e.g., CES-C and NOESM) simply produce an increase in the eastward transport of moisture, whereas some models (e.g., BCCCS, INM-A and CMCC) simulate the increase in the north-eastward transport over the whole of West

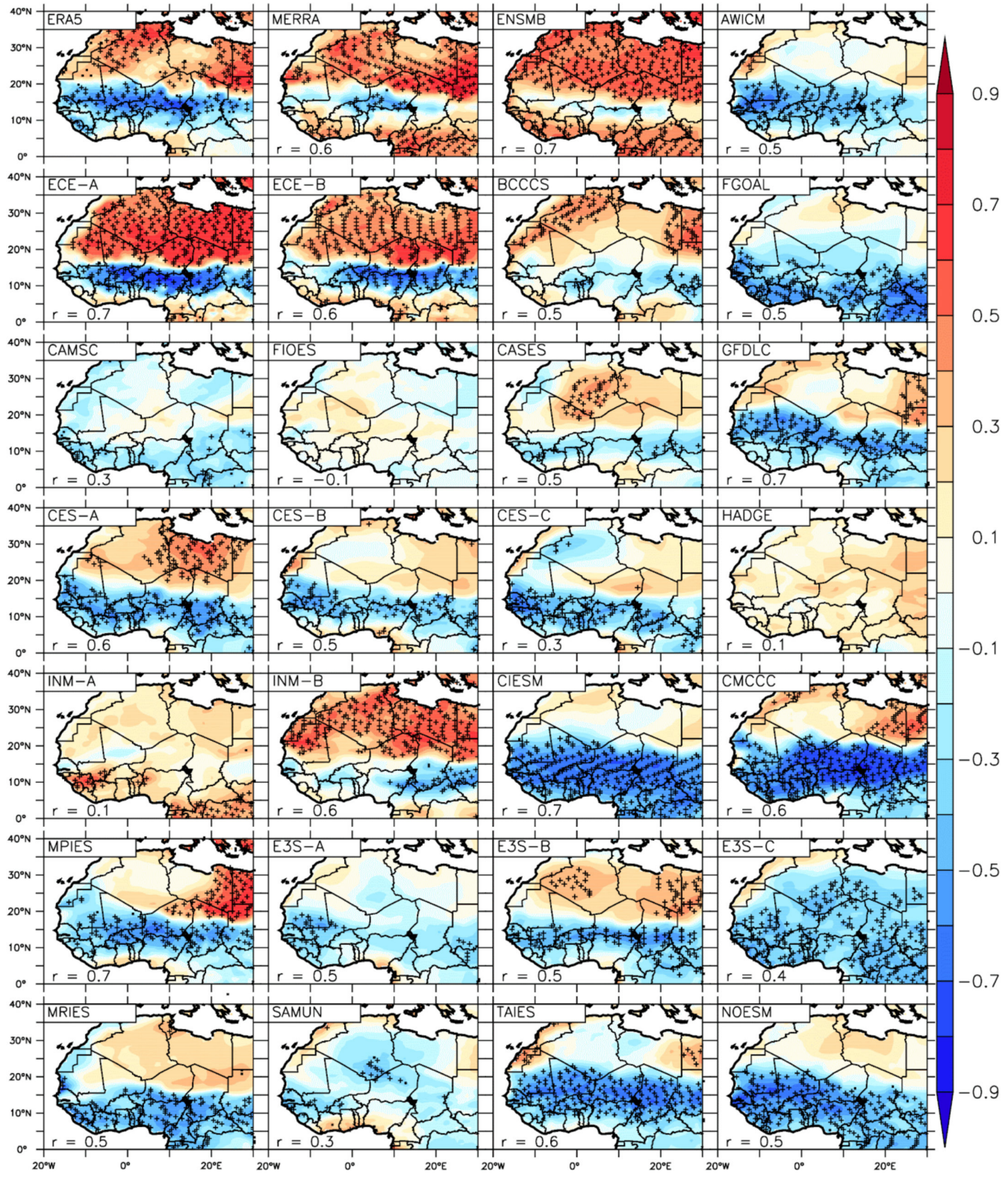

FIGURE 7 | The spatial distribution of correlation between the WAWJ strength ($m\,s^{-1}$; averaged over the jet core area; white boxes in Figure 3) and temperature (°C) over West Africa in August (1980–2014), as observed by ERA5 (WAWJ) and MERRA (WAWJ) with CRU (temperature) and simulated by the CMIP6 models and the multi-model ensemble mean. The similarity between the simulated and observed patterns is quantified and indicated with spatial correlation in each panel, and significance at each grid box at a 95% confidence level is marked with a (+) symbol. [Colour figure can be viewed at wileyonlinelibrary.com]

Africa, and some models (E3S-A and E3S-C) do not produce any coherent pattern in moisture transport over the domain (Figure 8).

According to the spatial correlation coefficient, the simulations perform better at linking the jet with the spatial distribution of temperature than with the spatial distribution of precipitation

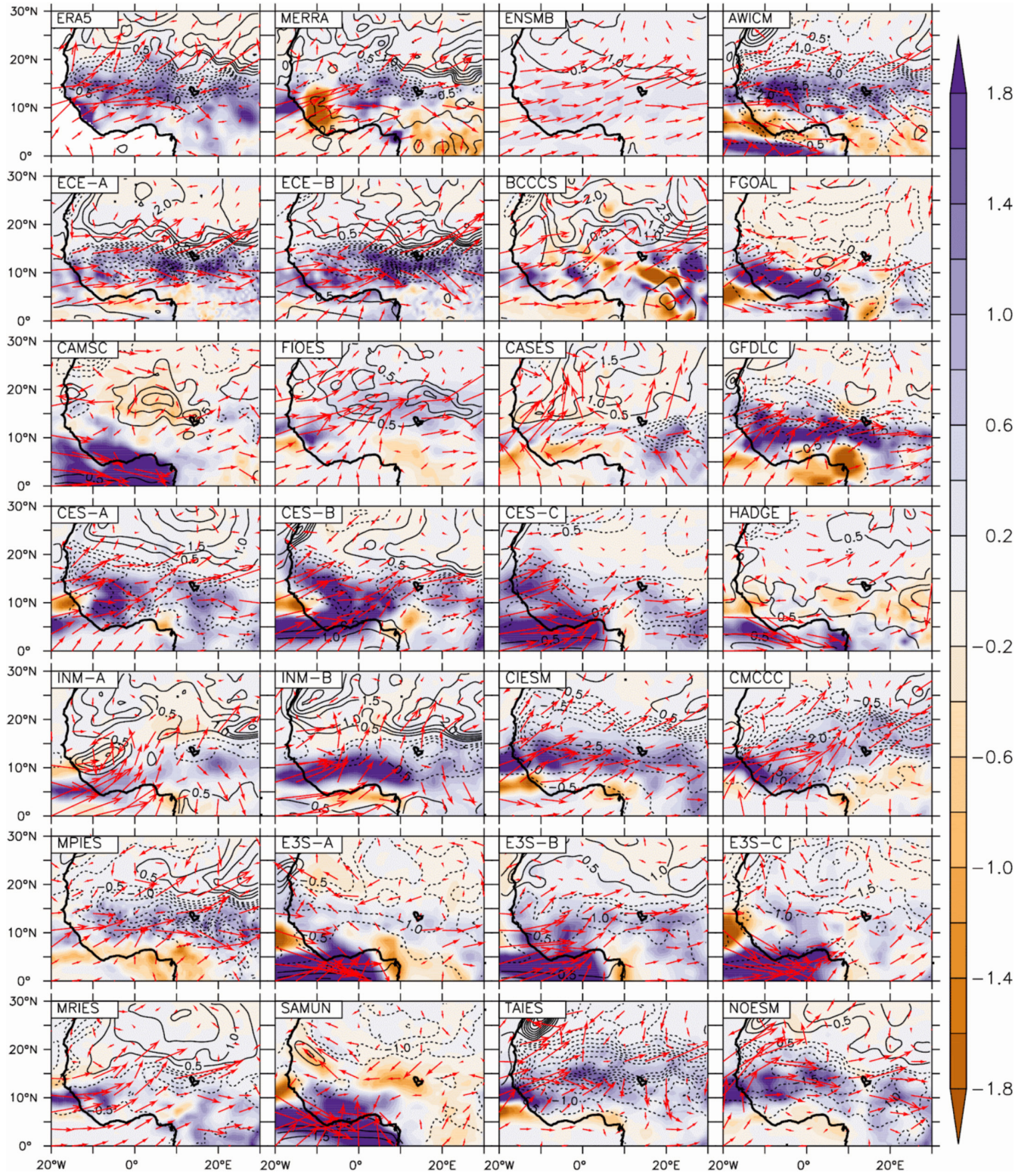

FIGURE 8 | Difference of the composite of precipitation (mm/mon; shading), temperature (°C; contour), and moisture flux (vectors; 925 hPa) anomalies during positive and negative modes of WAWJ (1980–2014) as observed in ERA5 and MERRA (with CRU precipitation) and simulated by CMIP6 models and the multi-model ensemble mean. [Colour figure can be viewed at wileyonlinelibrary.com]

(Figure 7). Only 7 models (28%) show a weak agreement ($r < 0.5$) with ERA5 results, namely: FIOES ($r = -0.1$), HADGE ($r = 0.1$), INM-A ($r = 0.1$), CAMSC ($r = 0.3$), CES-C ($r = 0.3$), SAMUN ($r = 0.3$) and E3S-C ($r = 0.4$). Although HADGE and INM-A show a positive correlation between the jet and the spatial distribution of temperature over most parts of the domain, E3S-C shows a positive correlation. CAMSC features a dipole correlation, but it features some positive correlations north of 20 °N in contrast to the ERA5 result. Not all the models that have good agreement with ERA5 (i.e., $0.5 \leq r \leq 0.7$)

reproduce the dipole correlation pattern as in ERA5. For instance, 6 models (AWICM, FGOAL, E3S-A, E3S-C, TAIES and NOESM) show very weak positive correlations ($r < 0.3$) between the jet and temperature north of 25° N. This suggests that these models may underestimate the link between WAWJ and the SHL. However, ECE-A and ECE-B show the best agreement with ERA5 on the relationship between WAWJ and the spatial distribution of temperature and precipitation over the sub-continent. Though the ensemble mean agrees with the observations that the stronger WAWJ transports moisture into the subcontinent and more moisture north-eastward into the Sahel. However, it shows weak links between the jet and the temperature and precipitation.

3.6 | WAWJ-Sahel Precipitation Relationship and Model Biases

The previous section has indicated the strong role of the WAWJ in precipitation variability and that there are large variations between models in their ability to represent this. We now explore the relationship between the WAWJ-precipitation correlation and the models' precipitation biases over the Sahel (Figure 9). The figure reveals an association between the models' depiction of the WAWJ-precipitation relationship and the magnitude of biases in Sahel precipitation. Models that exhibit stronger correlations between the WAWJ and Sahel precipitation tend to display lower precipitation biases over the Sahel compared to models with weaker correlations. This finding supports the conclusions of previous literature (e.g., drawn by Tamoffo et al. 2023), who argue that the inaccuracies in modelled precipitation over West Africa, particularly in the Sahel, stem from the models' limited ability to accurately simulate the strength of processes, such as the WAWJ, which play a crucial role in advecting moisture into the subcontinent.

It has been suggested that higher resolution models may be necessary to adequately simulate Sahel precipitation (e.g., Vellinga et al. 2016; Birch and Parker 2014) and whilst this is not the focus of the present study, we briefly compare the CMIP6 models with 10 high-resolution HighResMIP CMIP6 models (Ajibola et al. 2020, 2022) and their ensemble mean (Appendix S2, Figure A2). The HighResMIP models still show a broad range in terms of the precipitation biases and the correlations between WAWJ and Sahel precipitation. As for the coarser resolution models, there is a slight tendency for the models with higher correlation scores to show smaller biases, however, some of the HighResMIP models with good correlation scores still have biases more than 50 mm month (an analysis of the structure of the WAWJ in HighResMIP models also showed a range of behaviours across models and does not indicate a jump in performance relative to CMIP6; Appendix S2, Figure A2).

The correlation between WAWJ strength and Sahel precipitation could serve as a valuable metric for both evaluating and improving the performance of CMIP6 models. In model development, tracking the representation of the WAWJ and its linkage to rainfall could be a useful diagnostic. Figure 9 clearly shows that a strong relationship between WAWJ and rainfall is not a sufficient condition for a small precipitation bias, but it might be necessary to achieve a very low bias and to simulate the regional circulation. Analysis of the WAWJ and linkages to rainfall could also be useful for investigating future projections, particularly as many models show drying over the west of the Sahel, in close proximity to the WAWJ (Audu et al. 2024; Monerie et al. 2020).

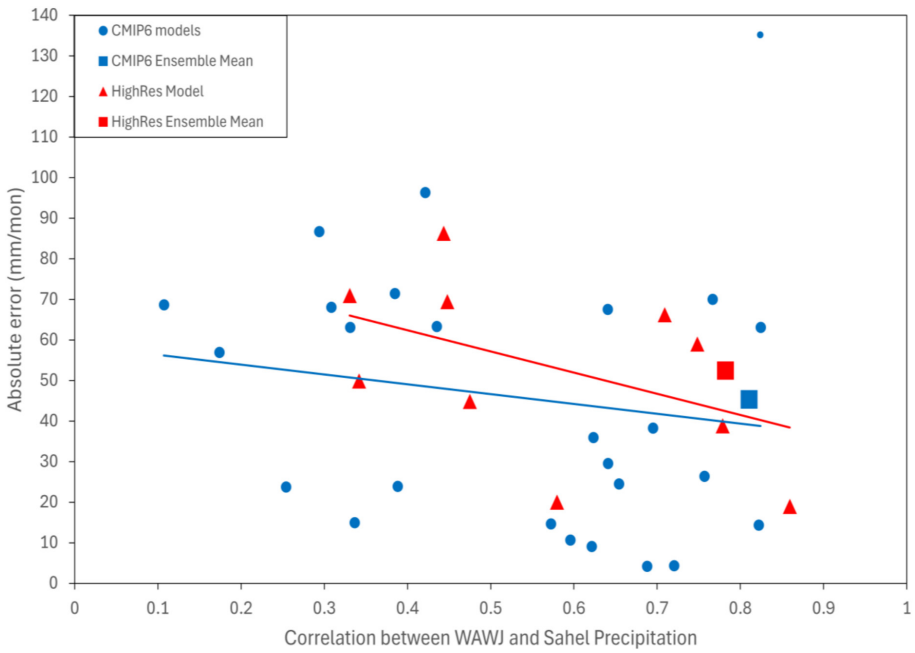

FIGURE 9 | The relationship between WAWJ strength and Sahel precipitation in CMIP6 models versus the models' weakness (absolute error) in simulating Sahel precipitation (with reference to CRU). The WAWJ-Sahel rainfall relationship is quantified with correlation (horizontal axis). The blue circles and squares represent the 25 models in Table 1 and their ensemble mean, respectively. Also, the red triangles and squares represent 10 high-resolution CMIP6 models (see Appendix S2) and their ensemble mean, respectively. [Colour figure can be viewed at wileyonlinelibrary.com]

4 | Conclusion

As part of the ongoing efforts to improve the simulation and projection of precipitation in the Sahel, this study has evaluated the capability of CMIP6 models in simulating the West African Westerly Jet (WAWJ) and its influence on Sahel precipitation. The study analysed CRU, ERA5, MERRA, CFSR (Supporting Information) and 25 CMIP6 datasets for a period of 35 years. The study, which defined WAWJ as a low-level westerly jet over the eastern Atlantic and the West African coast, compared the characteristics of WAWJ in the reanalysis (primarily ERA5, with MERRA used for cross-validation and CFSR presented in the Supporting Information) and the CMIP6 and used standard statistical metrics to quantify the comparison. It also quantifies the relationship between the jet and climate variables in the datasets with correlation analysis and uses composite analysis of the climate variables during the positive and negative modes of WAWJ to investigate the relationship. The results of the study can be summarised below:

- ERA5 and MERRA show that the WAWJ has its core at 925 hPa and attains its maximum speed in August. Most CMIP6 simulations broadly capture the annual cycle and vertical and horizontal structure of the jet, but produce jets that develop too early and are too strong with reference to ERA5 results.
- Although most CMIP6 models agree with the reanalysis on the spatial structure of WAWJ (covering 6° N–12° N, 15° W—35° W with the core around 8° N and 20° W), more than 39.5% disagree with ERA5 on the spatial structure. Some of the models show the WAWJ further north or south, or with a different spatial or vertical extent. This appears to relate to the representation of other features, including the ITCZ, the Saharan Heat Low and the African Easterly Jet.
- Most of the models reproduce a positive trend in the strength of WAWJ as in ERA5 results, but some models show a negative trend in the jet's strength.
- In ERA5 and MERRA, the WAWJ has a strong positive correlation with precipitation over West Africa (especially over the Sahel) and a dipole correlation pattern with temperature over the sub-continent. The spatial correlation between ERA5 and MERRA for near-surface temperature patterns is $r \approx 0.6$, indicating moderate agreement between the two reanalyses despite some latitudinal shifts. Most CMIP6 simulations capture the correlation between the jet and temperature, but only a few of them capture the correlation between the jet and precipitation.
- A stronger WAWJ transports more moisture eastward into the continent, providing more moisture for the north-eastward transport into the Sahel. However, when the models have a strong WAWJ, they don't consistently show enhancement of both the eastward and north-eastward transports. In addition, some of the models which do capture moisture flux increases during a strong WAWJ fail to translate the increase in moisture transport to a commensurable increase in precipitation in the Sahel.
- The majority of the CMIP6 models which simulate a weak relationship between WAWJ and Sahel precipitation show large biases in precipitation over the Sahel region.

This study makes a contribution to the literature about the simulation of the West African climate, highlighting the importance and potential value in evaluating the WAWJ. Clearly, CMIP models have large persistent biases over West Africa. Some literature suggests that it may be necessary to substantially increase resolution and run models in convection-permitting mode in order to improve the simulation of the monsoon (Birch and Parker 2014; Berthou et al. 2019). However, these models require vast computing resources and it may be a long time before we are able to generate an ensemble of runs that can be used to investigate uncertainty in future climate change. In the meantime, CMIP models remain the primary tool for investigating future climate and informing adaptation (either directly or as input to regional climate models or statistical downscaling approaches). A better understanding of how models represent regional circulation features can both inform model development and provide insights about whether and how the model results can be used for informing adaptation. For example, this study could be used to identify which models have a better representation of the WAWJ and Sahel precipitation, and to help interpret future projections over the region. In general, they indicate that we should be cautious about using these models to represent precipitation variability and change over West Africa.

To aid model evaluation and development and future research, we have made a diagnostic of the WAWJ available via GitHub (https://github.com/Priority-on-African-Diagnostics/LaunchPAD/tree/master/DIAGNOSTICS/West_African_Westerly_Jet). The study also indicates some fruitful areas for further research. The relative performance of the models may depend on the horizontal resolution. Although the formation of WAWJ is closely related to the strength and westward extension of the SHL (Pu and Cook 2010), improvement in simulated SHL is linked to an adequate representation of the complex topography of Africa (Diallo et al. 2014). Hence, changes in model resolution may improve the performance of models in simulating WAWJ. Although our brief analysis suggests that HighResMIP models do not substantially improve the simulation, future studies could investigate in more depth how the results of this study are sensitive to model resolution and representation of topography. In addition, the biases identified in some of the models in this study could be related to physics parameterisation (Nicholson 2018). For example, the inability of some of the models to translate the moisture transport by the jet into commensurable precipitation suggests that the convective parameterisation schemes in the models might be too weak in translating the excess moisture into precipitation. Therefore, future studies could evaluate different physics parameterisation schemes in those models. Lastly, this study has further established that the jet transports moisture into the region, but that may not be a sufficient criterion for rainfall occurrence. Investigating how well the simulations simulate various processes that trigger deep convection in relation to the westerly moisture flux over West Africa would be very useful.

Author Contributions

All authors contributed to the study conception and methodology. The first author prepared the material, collected the data and performed

the analysis under the supervision of the second author. The first draft of the manuscript was written by the first author and all other authors were responsible for reviewing and editing previous versions of the manuscript. All authors read and approved the final manuscript.

Acknowledgements

We sincerely thank LaunchPAD (Priority on African Diagnostic) and the team for creating the Climate Model Evaluation Hub for Africa and the Foreign, Commonwealth & Development Office (FCDO) for the financial support. This work is also supported by the National Research Foundation of South Africa (Reference Number: RPOAM231218201502) and by the Pan-African and Transdisciplinary Lens in the Margins: Tackling the Risks of Extreme Events (PALM-TREEs) project (Grant no. 110002-002; funded by the International Development Research Centre and the Foreign, Commonwealth & Development Office).

Funding

This work was supported by LaunchPAD (funded by Foreign, Commonwealth & Development Office (FCDO)), National Research Foundation of South Africa (NRF; Reference Number: RPOAM231218201502) and Pan-African and Transdisciplinary Lense in the Margins: Tackling the Risks of Extreme Event (PALM-TREEs) project (Grant no. 110002-002; funded by the International Development Research Centre and the Foreign, Commonwealth & Development Office).

Conflicts of Interest

The authors declare no conflicts of interest.

Data Availability Statement

The code for the diagnostic is made available at https://github.com/Priority-on-African-Diagnostics/LaunchPAD.

References

Aadhar, S., and V. Mishra. 2020. "On the Projected Decline in Droughts Over South Asia in CMIP6 Multimodel Ensemble." *Journal of Geophysical Research* 125, no. 20: 33587. https://doi.org/10.1029/2020jd033587.

Ajibola, F. O., B. Zhou, S. Shahid, and M. A. Ali. 2022. "Performance of CMIP6 HighResMIP Simulations on West African Drought." *Frontiers of Earth Science in China* 10: 1–13. https://doi.org/10.3389/feart.2022.925358.

Ajibola, F. O., B. Zhou, G. Tchalim Gnitou, and A. Onyejuruwa. 2020. "Evaluation of the Performance of CMIP6 HighResMIP on West African Precipitation." *Atmosphere* 11, no. 10: 1053.

Almazroui, M., F. Saeed, S. Saeed, et al. 2020. "Projected Change in Temperature and Precipitation Over Africa From CMIP6." *Earth Systems and Environment* 4, no. 3: 455–475.

Ankidawa, B. A., J. M. Ishaku, and A. A. Hassan. 2018. "Estimation of Aquifer Transmissivity Using Dar Zarrouk Parameters Derived From Resistivity Soundings on the Floodplain of River Dadin Kowa, Gombe State, Northeastern." Computational Engineering and. http://www.jcepm.com/article_82842.html.

Annor, T., A. T. Ackon, R. James, et al. 2023. "Heat Band, Rain Band and Heat Low Migration: Process-Based Evaluation of Some CMIP6 GCMs Over West Africa." *Climate Dynamics* 62: 791–806. https://doi.org/10.1007/s00382-023-06930-4.

Audu, E. O., R. D. Dixon, and I. Diallo. 2024. "Understanding the Zonal Variability in Projections of Sahel Precipitation." *Geophysical Research Letters* 51, no. 20: 1–10. https://doi.org/10.1029/2024gl110177.

Bader, D. C., R. Leung, M. Taylor, and R. B. McCoy. 2019a. "E3SM-Project E3SM1.0 Model Output Prepared for CMIP6 CMIP Historical [Data Set]." Earth System Grid Federation. https://doi.org/10.22033/ESGF/CMIP6.4497.

Bader, D. C., R. Leung, M. Taylor, and R. B. McCoy. 2019b. "E3SM-Project E3SM1.1 Model Output Prepared for CMIP6 CMIP Historical [Data Set]." Earth System Grid Federation. https://doi.org/10.22033/ESGF/CMIP6.11485.

Bader, D. C., R. Leung, M. Taylor, and R. B. McCoy. 2020. "E3SM-Project E3SM1.1ECA Model Output Prepared for CMIP6 CMIP Historical [Data Set]." Earth System Grid Federation. https://doi.org/10.22033/ESGF/CMIP6.11486.

Bain, C. L., K. D. Williams, S. F. Milton, and J. T. Heming. 2014. "Objective Tracking of African Easterly Waves in Met Office Models." *Quarterly Journal of the Royal Meteorological Society* 140, no. 678: 47–57. https://doi.org/10.1002/qj.2110.

Balme, M., T. Vischel, T. Lebel, C. Peugeot, and S. Galle. 2006. "Assessing the Water Balance in the Sahel: Impact of Small Scale Rainfall Variability on Runoff: Part 1: Rainfall Variability Analysis." *Journal of Hydrology* 331, no. 1–2: 336–348.

Basutti, M. 2019. "Rainfall Trends in the African Sahel: Characteristics, Processes, and Causes." *Wiley Interdisciplinary Reviews: Climate Change* 10, no. 4: e591.

Becker, A., P. Finger, A. Meyer-Christoffer, et al. 2013. "A Description of the Global Land-Surface Precipitation Data Products of the Global Precipitation Climatology Centre With Sample Applications Including Centennial (Trend) Analysis From 1901–Present." *Earth System Science Data* 5, no. 1: 71–99. https://doi.org/10.5194/essd-5-71-2013.

Bercos-Hickey, E., and C. M. Patricola. 2021. "Anthropogenic Influences on the African Easterly Jet–African Easterly Wave System." *Climate Dynamics* 57, no. 9: 2779–2792. https://doi.org/10.1007/s00382-021-05838-1.

Berthou, S., D. P. Rowell, E. J. Kendon, et al. 2019. "Improved Climatological Precipitation Characteristics Over West Africa at Convection-Permitting Scales." *Climate Dynamics* 53, no. 3–4: 1991–2011. https://doi.org/10.1007/s00382-019-04759-4.

Biasutti, M. 2013. "Forced Sahel Rainfall Trends in the CMIP5 Archive." *Journal of Geophysical Research: Atmospheres* 118, no. 4: 1613–1623.

Birch, C., and D. Parker. 2014. "A Seamless Assessment of the Role of Convection in the Water Cycle of the West African Monsoon." *Journal of Geophysical Research: Atmospheres* 119: 2890–2912. https://doi.org/10.1002/2013JD020887.

Buontempo, C., B. Booth, and W. Moufouma-Okia. 2012a. "The Climate of the Sahel. Organisation for Economic Co-Operation and Development (OECD)." https://doi.org/10.1787/9789264171848-4-en.

Buontempo, C., B. Booth, and W. Moufouma-Okia. 2012b. "The Climate of the Sahel." 57. West African Studies Global Security Risks and West Africa Development Challenges: Development Challenges.

Chai, Z. 2020. "CAS CAS-ESM1.0 MODel Output Prepared for CMIP6 CMIP Historical [Data Set]." Earth System Grid Federation. https://doi.org/10.22033/ESGF/CMIP6.3353.

Cook, K. H., and E. K. Vizy. 2006. "Coupled Model Simulations of the West African Monsoon System: Twentieth-And Twenty-First-Century Simulations." *Journal of Climate* 19, no. 15: 3681–3703.

Danabasoglu, G. 2019a. "CMIP6.CMIP.NCAR.CESM2-WACCM. Historical [Data Set]." Earth System Grid Federation. https://doi.org/10.22033/ESGF/CMIP6.10071.

Danabasoglu, G. 2019b. "NCAR CESM2 Model Output Prepared for CMIP6 CMIP Historical [Data Set]." Earth System Grid Federation. https://doi.org/10.22033/ESGF/CMIP6.7627.

Datti, A. D., G. Zeng, E. Tarnavsky, et al. 2024. "Evaluation of SATellite-Based Rainfall Estimates Against Rain Gauge Observations Across Agro-Climatic Zones of Nigeria, West Africa." *Remote Sensing* 16, no. 10: 1755. https://doi.org/10.3390/rs16101755.

Diallo, I., C. L. Bain, A. T. Gaye, et al. 2014. "Simulation of the West African Monsoon Onset Using the HadGEM3-RA Regional Climate Model." *Climate Dynamics* 43, no. 3-4: 575u2013594. https://doi.org/10.1007/s00382-014-2219-0.

Dixon, R. D., A. S. Daloz, D. J. Vimont, and M. Biasutti. 2017. "Saharan Heat Low Biases in CMIP5 Models." *Journal of Climate* 30, no. 8: 2867–2884. https://doi.org/10.1175/JCLI-D-16-0134.1.

Dixon, R. D., D. J. Vimont, and A. S. Daloz. 2018. "The Relationship Between Tropical Precipitation Biases and the Saharan Heat Low Bias in CMIP5 Models." *Climate Dynamics* 50, no. 9: 3729–3744. https://doi.org/10.1007/s00382-017-3838-z.

Dosio, A., M. W. Jury, M. Almazroui, et al. 2021. "Projected Future Daily Characteristics of African Precipitation Based on Global (CMIP5, CMIP6) and Regional (CORDEX, CORDEX-CORE) Climate Models." *Climate Dynamics* 57, no. 11: 3135–3158. https://doi.org/10.1007/s00382-021-05859-w.

EC-Earth. 2019. "EC-Earth-Consortium EC-Earth3 Model Output Prepared for CMIP6 CMIP Historical Dataset." Earth System Grid Federation. https://doi.org/10.22033/ESGF/CMIP6.4700.

EC-Earth-Veg. 2019. "EC-Earth-Consortium EC-Earth3-Veg Model Output Prepared for CMIP6 CMIP Historical [Data Set]." Earth System Grid Federation. https://doi.org/10.22033/ESGF/CMIP6.4706.

Ehsan, M. A., D. Nicolì, F. Kucharski, et al. 2020. "Atlantic Ocean Influence on Middle East Summer Surface Air Temperature." *NPJ Climate and Atmospheric Science* 3, no. 1: 1–8. https://doi.org/10.1038/s41612-020-0109-1.

Foltz, G. R., P. Brandt, I. Richter, et al. 2019. "The Tropical Atlantic Observing System." *Frontiers in Marine Science* 6: 206.

Geist, H. J., and E. F. Lambin. 2004. "Dynamic Causal Patterns of Desertification." *Bioscience* 54, no. 9: 817–829.

Giannini, A., M. Biasutti, and M. M. Verstraete. 2008. "A Climate Model-Based Review of Drought in the Sahel: Desertification, the Re-Greening and Climate Change." *Global and Planetary Change* 64, no. 3: 119u2013128. https://doi.org/10.1016/j.gloplacha.2008.05.004.

Grist, J. P., and S. E. Nicholson. 2001. "A Study of the Dynamic Factors Influencing the Rainfall Variability in the West African Sahel." *Journal of Climate* 14, no. 7: 1337–1359.

Grodsky, S. A., J. A. Carton, and S. Nigam. 2003. "Near Surface Westerly Wind Jet in the Atlantic ITCZ." *Geophysical Research Letters* 30, no. 19: 1–4.

Guo, H., J. G. John, C. Blanton, et al. 2018. "NOAA-GFDL GFDL-CM4 Model Output Historical [Data Set]." Earth System Grid Federation. https://doi.org/10.22033/ESGF/CMIP6.8594.

Hagos, S. M., and K. H. Cook. 2008. "Ocean Warming and Late-Twentieth-Century Sahel Drought and Recovery." *Journal of Climate* 21, no. 15: 3797–3814.

Harris, I., T. J. Osborn, P. Jones, and D. Lister. 2020. "Version 4 of the CRU TS Monthly High-Resolution Gridded Multivariate Climate Dataset." *Scientific Data* 7, no. 1: 109.

Hersbach, H., B. Bell, P. Berrisford, et al. 2019. "ERA5 Monthly Averaged Data on Single Levels From 1979 to Present, Copernicus Climate Change Service (C3S) Climate Data Store (CDS)."

Hourdin, F., A. Găinusă-Bogdan, P. Braconnot, J. L. Dufresne, A. K. Traore, and C. Rio. 2015a. "Air Moisture Control on Ocean Surface Temperature, Hidden Key to the Warm Bias Enigma." *Geophysical Research Letters* 42, no. 24: 10–885.

Hourdin, F., A. Găinusă-Bogdan, P. Braconnot, J.-L. Dufresne, A.-K. Traore, and C. Rio. 2015b. "Air Moisture Control on Ocean Surface Temperature, Hidden Key to the Warm Bias Enigma." *Geophysical Research Letters* 42, no. 24: 10,885–10,893.

Huang, W. 2019. "THU CIESM Model Output Prepared for CMIP6 CMIP Historical [Data Set]." Earth System Grid Federation. https://doi.org/10.22033/ESGF/CMIP6.8843.

Iyakaremye, V., G. Zeng, A. Siebert, and X. Yang. 2021. "Contribution of External Forcings to the Observed Trend in Surface Temperature Over Africa During 1901–2014 and Its Future Projection From CMIP6 Simulations." *Atmospheric Research* 254: 105512.

James, R., R. Washington, B. Abiodun, et al. 2018. "Evaluating Climate Models With an African Lens." *Bulletin of the American Meteorological Society* 99, no. 2: 313–336. https://doi.org/10.1175/BAMS-D-16-0090.1.

Jnr, S. D. 2014. "Land Degradation and Agriculture in the Sahel of Africa: Causes, Impacts and Recommendations." *Journal of Agricultural Science and Applications* 3, no. 3: 67–73.

Jung, T., L. Ferranti, and A. M. Tompkins. 2006. "Response to the Summer of 2003 Mediterranean SST Anomalies Over Europe and Africa." *Journal of Climate* 19, no. 20: 5439–5454. https://doi.org/10.1175/JCLI3916.1.

Jungclaus, J., M. Bittner, K.-H. Wieners, et al. 2019. "MPI-M MPI-ESM1.2-HR Model Output Prepared for CMIP6 CMIP Historical [Data Set]." Earth System Grid Federation. https://doi.org/10.22033/ESGF/CMIP6.6594.

Klutse, N. A. B., K. A. Quagraine, F. Nkrumah, et al. 2021. "The Climatic Analysis of Summer Monsoon Extreme Precipitation Events Over West Africa in CMIP6 Simulations." *Earth Systems and Environment* 5, no. 1: 25–41.

Kuete, G., W. P. Mba, R. James, E. Dyer, T. Annor, and R. Washington. 2022. "How Do Coupled Models Represent the African Easterly Jets and Their Associated Dynamics Over Central Africa During the September–November Rainy Season?" *Climate Dynamics* 60: 2907–2929. https://doi.org/10.1007/s00382-022-06467-y.

Lavaysse, C., C. Flamant, S. Janicot, et al. 2009. "Seasonal Evolution of the West African Heat Low: A Climatological Perspective." *Climate Dynamics* 33, no. 2: 313–330.

Lee, W.-L., and H.-C. Liang. 2020. "AS-RCEC TaiESM1.0 Model Output Prepared for CMIP6 CMIP Historical [Data Set]." Earth System Grid Federation. https://doi.org/10.22033/ESGF/CMIP6.9755.

Lele, M. I., and L. M. Leslie. 2016. "Intraseasonal Variability of Low-Level Moisture Transport Over West Africa." *Climate Dynamics* 47, no. 11: 3575–3591.

Li, J., Z. Sun, Y. Liu, Q. You, G. Chen, and Q. Bao. 2021. "Top-Of-Atmosphere Radiation Budget and Cloud Radiative Effects Over the Tibetan Plateau and Adjacent Monsoon Regions From CMIP6 Simulations." *Journal of Geophysical Research* 126, no. 9: 345. https://doi.org/10.1029/2020jd034345.

Liu, W., K. H. Cook, and E. K. Vizy. 2020. "Role of the West African Westerly Jet in the Seasonal and Diurnal Cycles of Precipitation Over West Africa." *Climate Dynamics* 54, no. 1–2: 843–861.

Lovato, T., and D. Peano. 2020. "CMCC CMCC-CM2-SR5 Model Output Prepared for CMIP6 CMIP Historical [Data Set]." Earth System Grid Federation. https://doi.org/10.22033/ESGF/CMIP6.3825.

Maidment, R. I., D. I. F. Grimes, R. P. Allan, H. Greatrex, O. Rojas, and O. Leo. 2013. "Evaluation of Satellite-Based and Model Re-Analysis Rainfall Estimates for Uganda: Evaluation of Rainfall Estimates for Uganda." *Meteorological Applications* 20, no. 3: 308–317. https://doi.org/10.1002/met.1283.

Monerie, P. A., C. M. Wainwright, M. Sidibe, and A. A. Akinsanola. 2020. "Model Uncertainties in Climate Change Impacts on Sahel Precipitation in Ensembles of CMIP5 and CMIP6 Simulations." *Climate Dynamics* 55, no. 5: 1385–1401.

Nicholson, S. E. 2013. "The West African Sahel: A Review of Recent Studies on the Rainfall Regime and Its Interannual Variability." *ISRN Meteorology* 2013: 1–32.

Nicholson, S. E. 2018. "The ITCZ and the Seasonal Cycle Over Equatorial Africa." *Bulletin of the American Meteorological Society* 99, no. 2: 337–348. https://doi.org/10.1175/bams-d-16-0287.1.

Nicholson, S. E., C. Funk, and A. H. Fink. 2018. "Rainfall Over the African Continent From the 19th Through the 21st Century." *Global and Planetary Change* 165: 114–127. https://doi.org/10.1016/j.gloplacha.2017.12.014.

Park, S., and J. Shin. 2019. "SNU SAM0-UNICON Model Output Prepared for CMIP6 CMIP Historical [Data Set]." Earth System Grid Federation. https://doi.org/10.22033/ESGF/CMIP6.7789.

Pu, B., and K. H. Cook. 2010. "Dynamics of the West African Westerly Jet." *Journal of Climate* 23, no. 23: 6263–6276.

Pu, B., and K. H. Cook. 2012. "Role of the West African Westerly Jet in Sahel Rainfall Variations." *Journal of Climate* 25, no. 8: 2880–2896.

Quagraine, K. A., F. Nkrumah, C. Klein, N. A. B. Klutse, and K. T. Quagraine. 2020. "West African Summer Monsoon Precipitation Variability as Represented by Reanalysis Datasets." *Climate* 8, no. 10: 111.

Ridley, J., M. Menary, T. Kuhlbrodt, M. Andrews, and T. Andrews. 2019. "MOHC HadGEM3-GC31-LL Model Output Prepared for CMIP6 CMIP Historical [Data Set]." Earth System Grid Federation. https://doi.org/10.22033/ESGF/CMIP6.6109.

Roberts, A. J., J. H. Marsham, and P. Knippertz. 2015. "Disagreements in Low-Level Moisture Between (Re)analyses Over Summertime West Africa." *Monthly Weather Review* 143, no. 4: 1193–1211. https://doi.org/10.1175/mwr-d-14-00218.1.

Robertson, F. R., M. G. Bosilovich, and J. B. Roberts. 2016. "Reconciling Land / Ocean Moisture Transport Variability in Reanalyses With P-ET in Observationally-Driven Land Surface Models." *Journal of Climate* 29, no. 23: 8625–8646. https://doi.org/10.1175/JCLI-D-16-0379.1.

Roehrig, R., D. Bouniol, F. Guichard, F. Hourdin, and J. L. Redelsperger. 2013. "The Present and Future of the West African Monsoon: A Process-Oriented Assessment of CMIP5 Simulations Along the AMMA Transect." *Journal of Climate* 26, no. 17: 6471–6505.

Rong, X. 2019. "CAMS CAMS_CSM1.0 Model Output Prepared for CMIP6 CMIP Historical [Data Set]." Earth System Grid Federation. https://doi.org/10.22033/ESGF/CMIP6.9754.

Rowell, D. P. 2003. "The Impact of Mediterranean SSTs on the Sahelian Rainfall Season." *Journal of Climate* 16, no. 5: 849–862.

Seland, Ø., M. Bentsen, D. Olivié, et al. 2020. "Overview of the Norwegian Earth System Model (NorESM2) and Key Climate Response of CMIP6 DECK, Historical, and Scenario Simulations." *Geoscientific Model Development* 13, no. 12: 6165–6200. https://doi.org/10.5194/gmd-13-6165-2020.

Semmler, T., S. Danilov, T. Rackow, et al. 2018. "AWI AWI-CM1.1MR Model Output Prepared for CMIP6 CMIP Historical [Data Set]." Earth System Grid Federation. https://doi.org/10.22033/ESGF/CMIP6.2686.

Song, Z., F. Qiao, Y. Bao, Q. Shu, Y. Song, and X. Yang. 2019. "FIO-QLNM FIO-ESM2.0 Model Output Prepared for CMIP6 CMIP Historical [Data Set]." Earth System Grid Federation. https://doi.org/10.22033/ESGF/CMIP6.9199.

Stouffer, R. J., V. Eyring, G. A. Meehl, et al. 2017. "CMIP5 Scientific Gaps and Recommendations for CMIP6." *Bulletin of the American Meteorological Society* 98, no. 1: 95–105. https://doi.org/10.1175/bams-d-15-00013.1.

Tamoffo, A. T., L. K. Amekudzi, T. Weber, D. A. Vondou, E. I. Yamba, and D. Jacob. 2022. "Mechanisms of Rainfall Biases in Two CORDEX-CORE Regional Climate Models at Rainfall Peaks Over Central Equatorial Africa." *Journal of Climate* 35, no. 2: 639–668. https://doi.org/10.1175/JCLI-D-21-0487.1.

Tamoffo, A. T., A. Dosio, L. K. Amekudzi, and T. Weber. 2023. "Process-Oriented Evaluation of the West African Monsoon System in CORDEX-CORE Regional Climate Models." *Climate Dynamics* 60, no. 9: 3187–3210. https://doi.org/10.1007/s00382-022-06502-y.

Thorncroft, C. D., and M. Blackburn. 1999. "Maintenance of the African Easterly Jet." *Quarterly Journal of the Royal Meteorological Society* 125, no. 555: 763–786. https://doi.org/10.1002/qj.49712555502.

Tomalka, J., J. Birner, A. M. Dieye, et al. 2021. "Climate Risk Profile: Sahel. A Joint Publication by the Potsdam Institute for Climate Impact Research (PIK) and the United Nations High Commissioner for Refugees (UNHCR) Under the Predictive Analytics Project in Support of the United Nations Integrated Strategy for the Sahel (UNISS)." https://publications.pik-potsdam.de/pubman/faces/ViewItemFullPage.jsp?itemId=item_26168_1.

Trenberth, K. E., A. Dai, G. van der Schrier, et al. 2013. "Global Warming and Changes in Drought." *Nature Climate Change* 4, no. 1: 17–22.

Tschakert, P., R. Sagoe, G. Ofori-Darko, and S. N. Codjoe. 2010. "Floods in the Sahel: An Analysis of Anomalies, Memory, and Anticipatory Learning." *Climatic Change* 103, no. 3: 471–502.

Vellinga, M., M. Roberts, P. L. Vidale, et al. 2016. "Sahel Decadal Rainfall Variability and the Role of Model Horizontal Resolution." *Geophysical Research Letters* 43, no. 1: 326–333.

Vizy, E. K., and K. H. Cook. 2001. "Mechanisms by Which Gulf of Guinea and Eastern North Atlantic Sea Surface Temperature Anomalies Can Influence African Rainfall." *Journal of Climate* 14, no. 5: 795–821.

Vogel, L. 2010. "Food Crisis Escalates in Africa's Sahel Region." *CMAJ: Canadian Medical Association Journal* 182, no. 12: E555–E556. https://doi.org/10.1503/cmaj.109-3315.

Volodin, E., E. Mortikov, A. Gritsun, et al. 2019a. "INM INM-CM4-8 Model Output Prepared for CMIP6 CMIP Historical [Data Set]." Earth System Grid Federation. https://doi.org/10.22033/ESGF/CMIP6.5069.

Volodin, E., E. Mortikov, A. Gritsun, et al. 2019b. "INM INM-CM5-0 Model Output Prepared for CMIP6 CMIP Historical [Data Set]." Earth System Grid Federation. https://doi.org/10.22033/ESGF/CMIP6.5070.

Williams, K. D., C. M. Harris, A. Bodas-Salcedo, et al. 2015. "The Met Office Global Coupled Model 2.0 (GC2) Configuration." *Geoscientific Model Development Discussions* 8, no. 1: 521–565. https://doi.org/10.5194/gmdd-8-521-2015.

Wu, T., M. Chu, M. Dong, et al. 2018. "BCC BCC-CSM2MR Model Output Prepared for CMIP6 CMIP Historical [Data Set]." Earth System Grid Federation. https://doi.org/10.22033/ESGF/CMIP6.2948.

Yu, Y. 2019. "CAS FGOALS-f3-L Model Output Prepared for CMIP6 CMIP Historical [Data Set]." Earth System Grid Federation. https://doi.org/10.22033/ESGF/CMIP6.3355.

Yukimoto, S., T. Koshiro, H. Kawai, et al. 2019. "MRI MRI-ESM2.0 Model Output Prepared for CMIP6 CMIP Historical [Data Set]." Earth System Grid Federation. https://doi.org/10.22033/ESGF/CMIP6.6842.

Žagar, N., G. Skok, and J. Tribbia. 2011. "Climatology of the ITCZ Derived From ERA Interim Reanalyses." *Journal of Geophysical Research: Atmospheres* 116, no. D15: D15103. https://doi.org/10.1029/2011JD015695.

Supporting Information

Additional supporting information can be found online in the Supporting Information section. **Appendix S1:** joc70371-sup-0001-Appendix S1.docx. **Appendix S2:** joc70371-sup-0002-Appendix S2.docx.